Scanning Electron Microscopy

Volume 1986
Number 3 *Part III*

Article 6

7-29-1986

# Optical Microreflectometry and Microscopy of Chalcopyrite Specimens: Reflectance Calculation and Comparison to Backscattered Electron Microscopy

G. Remond
*Bureau de Recherches Géologiques et Minières*

R. Caye
*Bureau de Recherches Géologiques et Minières*

P. Ruzakowski
*University of Florida*

P. H. Holloway
*University of Florida*

SCANNING ELECTRON MICROSCOPY/1986/III (Pages 851-878)
SEM Inc., AMF O'Hare (Chicago), IL 60666-0507 USA

0586-5581/86$1.00+05

# OPTICAL MICROREFLECTOMETRY AND MICROSCOPY OF CHALCOPYRITE SPECIMENS : REFLECTANCE CALCULATION AND COMPARISON TO BACKSCATTERED ELECTRON MICROSCOPY

G. REMOND[1], R. CAYE[1], C. GATEAU[1], P. RUZAKOWSKI[2] and P.H. HOLLOWAY[2]

(1) Bureau de Recherches Géologiques et Minières
Département M.G.A. - 45060 ORLEANS, France
(2) Materials Science and Engineering Department, University of Florida
GAINESVILLE, FL 32611, USA

(Received for publication January 30, 1986, and in revised form July 29, 1986)

## Abstract

A model was developed to calculate the optical reflectance of an absorbing substrate covered by multiple thin layers of absorbing materials. Both multiple homogeneous thin layers and thin surface layers of mixed phases were modeled. Reflectance versus wavelength was measured for polished chalcopyrite ($CuFeS_2$) and compared to calculated data. The identity and thickness of surface compounds used to calculate reflectance curves were partially determined using X-ray photoelectron and Auger electron spectroscopies. Very good agreement between theoretical and experimental reflectance curves were observed as a function of surface composition. The hue (color) and luminosity (brightness) of the polished surface were also calculated from both experimental and theoretical curves and were found to also be valuable for evaluating surface composition. Contrast in optical photomicrographs resulting from both luminosity and hue was illustrated.

Secondary and backscattered electron microscopy were also used to image chalcopyrite polished surfaces which were naturally oxidized by an exposure before and after ion etching. For a substrate covered with thin layers, the resulting backscattered coefficient was calculated as a function of the backscattered coefficient for the surface and the substrate, respectively.

The variations of the relative difference between the effective backscattered coefficients vs the primary beam energy exhibited a maximum for a critical thickness difference of the surface layer. The dependence of the variations in thickness of the oxidized layer with the crystallographic orientation changes of the substrate as well as the resulting contrasts of the optical and electron images were discussed.

**Key Words : Optical Microreflectometry Reflectance Curves, Complex Refractive Index, Contrast, Hue, Luminosity, Secondary Electron Image, Backscattered Electron Image, Chalcopyrite.**

**Address for correspondence : G. REMOND
Bureau de Recherches Géologiques et Minières.
Département MGA. BP 6009
45060 ORLEANS Cedex,France.
(33) 38.64.31.24**

## Introduction

Optical microscopy has long been used to characterize mineral surfaces. In addition to using contrast changes from one mineral to another as a qualitative tool for analysis, reflectance vs. wavelength measurements (i.e.,reflectance curves) may be used to quantitatively identify the mineral and even measure the complex index of refraction for further identification (5).

However for reflectance measurements, the mineral specimen surface must be flat ; mechanical grinding followed by polishing is the most common technique to produce these flat surfaces. Because a variety of combinations of abrasives, suspension liquids (e.g., silicone oil, water, etc.) and media (e.g., metal foils, polishing cloth, etc.) are used for polishing, it is well known that reflectance curves vary with polishing technique. For example, Caye[5] has reported an absorption peak for cuprite ($Cu_2O$) polished with water on a soft cloth but no peak after polishing with silicone oil on an aluminium foil. Differences in the reflectance curves versus polishing procedure for chalcopyrite have been reported (25). In addition, Remond and coworkers have reported variability in EPMA data depending upon the sample preparation procedure (41). Surface-sensitive analytical techniques such as Electron Spectroscopy for Chemical Analysis (ESCA) and Auger electron spectroscopy (AES) have been used to study the surface composition of pyrite (39), chalcopyrite (26) (41), and sphalerite (37) (40). These data show that the changes in reflectance and EPMA data can result from thin surface layers resulting from chemical reactions before, during and after polishing.

In addition to observing changes in reflectance and EPMA data as a function of polishing procedure, changes versus time, temperature, and humidity have also been observed. Chen et al. (16) showed that an $Ag_2S$ film developed at the surface of chalcopyrite ($CuFeS_2$) and tennantite ($(Cu, Fe, Zn, Ag)_{12}(Sb, As)_4S_{13}$) minerals when native silver or silver-bearing minerals were present within the specimen. Remond et al. also showed that an $Ag_2S$ surface layer was formed on top of $CuFeS_2$ inclusions within an $Ag_2S$ matrix (36) (38), and that a copper sulfide layer developed on top of ZnS which was in contact with $CuFeS_2$ and bornite ($Cu_5FeS_4$) minerals (37) (40). Thus polished surfaces, especially after storage for some

time, may result in optical reflectance or EPMA data which are considerably different from those representative of the bulk mineral. It is the purpose of this research to understand the influence of surface composition upon the optical properties (reflectance, color, image) and electron absorption and emission (EPMA, secondary electron image). Specifically this initial report will discuss the influence of surface composition upon optical properties. To accomplish this, calculation of the reflectance of an absorbing substrate with absorbing or non-absorbing films will be derived. Complications resulting from anisotropic optical constants will be discussed, and the model calculations applied to chalcopyrite surfaces whose composition vary with polishing procedure and time. Finally optical contrast mechanisms are discussed and illustrated.

The existence of thin surface films also strongly influences the electron yield emission of a substrate (3) (27). Optical, secondary and backscattered images will be compared. Measurements of mass thickness surface films derived from backscattered electron emission have been already discussed (47). An effective backscattered electron coefficient will be calculated for a substrate covered with a thin film. The dependence of the effective backscattered coefficient to both the film thickness and primary electron beam energy will be illustrated. Sensitivity of optical microreflectometry and backscattered electron yield versus surface films will be illustrated for the case of oxide films on polished chalcopyrite specimens.

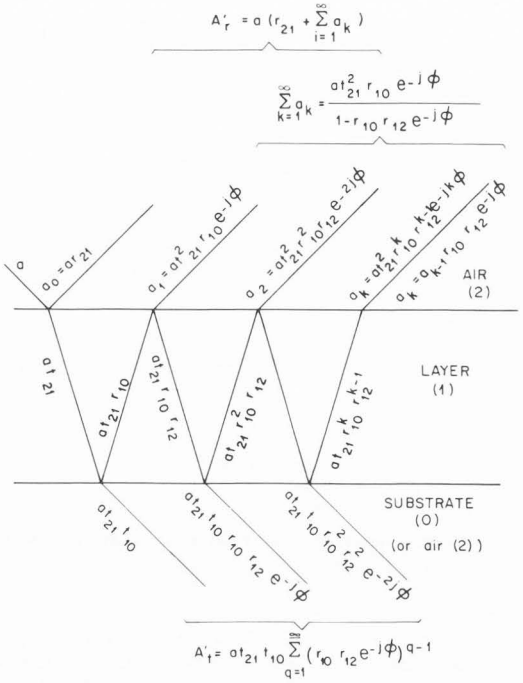


Fig. 1: Amplitudes of the reflected and transmitted waves through a thin absorbing layer.

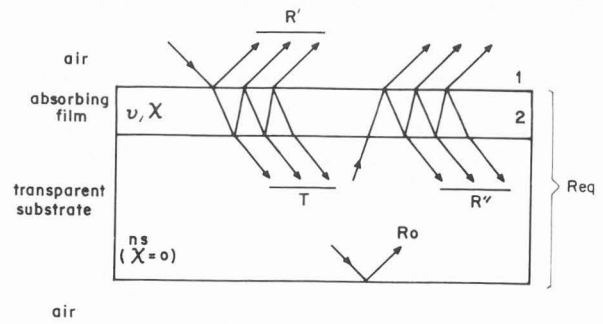


Fig. 2: Diagram illustrating the transmittance, T, the reflectances R,R', $R_o$ and Req used in eq. 15.

## Optical reflectance calculations for absorbing thin layers on a substrate

**Basis :** the basic equations for the optical reflectance with normally incident light have been already discussed for a **bulk** absorbing solid (22) (26), for an **unsupported** thin absorbing film (46) (47) and for thin films on transparent substrates (30) (31) (32). These results will be briefly reported before attempting to calculate the reflectance coefficient for thin films on **absorbing substrate.**

### Bulk material

Let a be the amplitude of the incident wave and $A_R$ the amplitude of the reflected light after being transmitted through a thin layer deposited at the surface of the substrate. Let $r_{ik}$ and $t_{ik}$ be the reflection and transmission coefficients respectively for the **amplitude** of the wave moving from the $i^{th}$ to the $k^{th}$ material. In cases of absorbing materials, these coefficients are complex and related by the following :

$$r_{ik} = -r_{ki} = \rho_{ik} e^{j\theta_{ik}} \qquad [1]$$

$$t_{ik} = t_{ki} = 1 - r_{ik}^2 \qquad [2]$$

The reflectance for the measured intensity is then given by:

$$R_{ik} = R_{ki} = r_{ik}\, r^*_{ki} = \rho_{ik}^2 \qquad [3]$$

where $r^*_{ik}$ is the complex conjugate of $r_{ik}$.

Considering only normally incident light, the reflectance may be expressed in terms of the refractive index, n, as:

$$r_{ik} = \frac{n_i - n_k}{n_i + n_k} \qquad [4]$$

For an absorbing material, n (= ν - j χ) is complex and includes the real refractive index, ν, and the extinction index, χ. Expressing $n_i$ and $n_k$ as complex terms, the reflectance is given by:

$$R_{ik} = \frac{(\nu_i - \nu_k)^2 + (\chi_i - \chi_k)^2}{(\nu_i + \nu_k)^2 + (\chi_i + \chi_k)^2} \qquad [5]$$

(The absorption coefficient, $k_i = \chi_i/\nu_i$, can be defined and equation [5] written entirely in terms of $\nu_i$ and $k_i$ if so desired). The phase change, $\theta_{ik}$, between the reflected and incident wave is given by:

$$\tan(\theta_{ik}) = \frac{2(\nu_i \chi_k - \nu_k \chi_i)}{(\nu_i^2 - \nu_k^2) + (\chi_i^2 - \chi_k^2)} \qquad [6]$$

The sign of $\tan(\theta_{ik})$ is defined by considering separately the two quantities $\sin\theta_{ik}$ and $\cos\theta_{ik}$ derived from the complex representation of the reflection coefficient ($r_{ik}$). The ranges of $\theta_{ik}$ are shown in Table 1 for various combination of values of the optical constants.

Note that when the index i refers to air ($\nu_i = 1$, $\chi_i = 0$), the phase change $\theta_{ik}$ due to reflection from an absorbing material ranges from $\pi/2$ to $\pi$. In the case of a transparent material ($\nu_k > 1$, $\chi_k = 0$) the phase change is equal to $\pi$.

Table 1 - Range of phase change versus complex optical constants of the substrate and surface layer.

| $\theta_{ik}$ | $\nu_i\chi_k > \nu_k\chi_i$ | $\nu_i\chi_k < \nu_k\chi_i$ |
|---|---|---|
| $\frac{\nu_i^2+\chi_i^2}{\nu_k^2+\chi_k^2} > 1$ | $0 < \theta_{ik} < \frac{\pi}{2}$ | $\frac{3\pi}{2} < \theta_{ik} < 2\pi$ |
| $\frac{\nu_i^2+\chi_i^2}{\nu_k^2+\chi_k^2} < 1$ | $\frac{\pi}{2} < \theta_{ik} < \pi$ | $\pi < \theta_{ik} < \frac{3\pi}{2}$ |

**Unsupported thin layer**

Assuming that the surfaces are perfectly parallel in the unsupported layer, transmitted wave amplitudes are shown in Fig. 1 where the optical refractive index may be different on one side of the layer versus the other side.

The complex amplitude of the wave reaching the detector is the sum of the amplitudes of all the successive reflected waves, $A_i^R$, which can be expressed by an arithmetical progression containing the factor $r_{21}r_{10}e^{-j\phi 1}$ where 2 denotes the incident medium, 1 denotes the layer and 0 denotes the transmission medium. The complex amplitude of the resulting reflected wave, $A'_R$, is:

$$A'_R = a\left[r_{21} + \frac{t_{21}\, r_{10}\, e^{-j\phi_1}}{1 - r_{12}\, r_{10}\, e^{-j\phi_1}}\right] \qquad [7]$$

or since $r_{12} = -r_{21}$ and $t_{21}^2 = 1 - r_{21}^2$

$$A'_R = a\frac{r_{21} + r_{10}e^{-j\varphi_1}}{1 + r_{21}\, r_{10}e^{-j\varphi_1}} = ar' = a\rho' e^{j\theta'} \qquad [8]$$

The complex amplitude of the resulting transmitted wave, $A'_T$, is thus:

$$A'_T = a\frac{t_{21}\, t_{10}}{1 + r_{21}\, r_{10}\, e^{-j\phi}} \qquad [9]$$

The argument $\phi_1$, expresses the phase change resulting from optical path differences through the layer of thickness d :

$$\varphi_1 = \frac{4\pi d_1(\nu_1 - j\chi_1)}{\lambda} \qquad [10]$$

The phase $\phi_1$ refers to the first reflected beam (see Fig. 1), where $\lambda$ is the wavelength of light. Phase changes upon reflection are contained within the complex reflection coefficient for the amplitude.

The total reflected intensity, $I_R$, and transmitted intensity, $I_T$, measured at the detectors are:

$$I_R = A'_R \cdot A'^*_R = a^2 R' \qquad [11]$$

$$I_T = A'_T \cdot A'^*_T = a^2 T' \qquad [12]$$

If the incident and transmission media are air, then:

$$R' = \left|\frac{r_{21} + r_{12}e^{-j\phi}}{1 + r_{21}r_{12}e^{-j\phi}}\right|^2 = \frac{R\left[(1-e^{-\frac{4\pi\chi d}{\lambda}})^2 + 4e^{-\frac{4\pi\chi d}{\lambda}}\sin^2\frac{2\pi}{\lambda}\nu d\right]}{(1-Re^{-\frac{4\pi\chi d}{\lambda}})^2 + 4Re^{-\frac{4\pi\chi d}{\lambda}}\sin^2(\theta + \frac{2\pi\nu d}{\lambda})} \qquad [13]$$

$$T = \left|\frac{t_{21}t_{12}}{1 + r_{21}r_{12}e^{-j\phi}}\right|^2 = \frac{e^{-\frac{4\pi\chi d}{\lambda}}\left[(1-R)^2 + 4R\sin^2\theta\right]}{(1-Re^{-\frac{4\pi\chi d}{\lambda}})^2 + 4Re^{-\frac{4\pi\chi d}{\lambda}}\sin^2(\theta + \frac{2\pi\nu d}{\lambda})} \qquad [14]$$

**Single or multiple homogeneous layer on a substrate**

For a transparent ($\chi = 0$) substrate, Buckley and Beaglehole (4) and Trodahl (48) showed that the reflectance coefficient was equal to the sum of the reflected **intensities** (considering multiple reflection and transmission) rather than their amplitudes. The resulting equivalent reflectance coefficient, Req, is given by:

$$Req = R + \frac{T^2 Ro}{1 - RoR'} \qquad [15]$$

where R' and T are the reflectance and transmission coefficients for the layer (equations [13] and [14]), and R" is the reflectance for light scattered from the substrate/layer interface after traveling through the substrate from back side illumination, and Ro is the reflectance of the light transmitted through the layer/substrate interface but reflected at the back surface of the finite transparent substrate (see Fig. 2). Thus, R' and R" are obtained by summing the amplitudes of the waves and are expressed by equations similar to equation [13]. Ro is given by:

$$Ro = \left[\frac{1-ns}{1+ns}\right]^2 \qquad [16]$$

where $n_s$ is the refractive index of the **transparent substrate.** The sum of intensities in equation [15] leads to much simpler expression than the equivalent to equation [7], but has a range of validity which varies with the thickness and nature of the layer and the substrate. Equation [15] is invalid for an absorbing substrate, since R" cannot be measured. Equations [8] and [11] therefore are complete formulation for the reflectance coefficient since the incident and transmission media against the layer may be different and the transmission medium may be either transparent or absorbing.

Substituting $r_{ik}$ from equation [5] and $\phi_1$ from equation [6] into equation [8], the amplitude of the total reflected wave is:

$$A'_R = a\,\frac{\rho_{21}e^{j\theta_{21}} + \rho_{10}e^{-\frac{4\Pi X_1 d_1}{\lambda}}e^{j(\theta_{10}-\frac{4\Pi\nu_1 d_1}{\lambda})}}{1+\rho_{21}\rho_{10}e^{-\frac{4\Pi X_1 d_1}{\lambda}}e^{j(\theta_{21}+\theta_{10}-\frac{4\Pi\nu_1 d_1}{\lambda})}} \qquad [17]$$

According to equation [11] the resulting reflectance coefficient, R', for the layer on a substrate is thus given by :

$$R' = \frac{R_{21}+R_{10}e^{-\frac{8\Pi X_1 d_1}{\lambda}} + 2\sqrt{R_{21}R_{10}}e^{-\frac{4\Pi X_1 d_1}{\lambda}}\cos(\theta_{21}-\theta_{10}+\frac{4\Pi\nu_1 d_1}{\lambda})}{1+R_{21}R_{10}e^{-\frac{8\Pi X_1 d_1}{\lambda}} + 2\sqrt{R_{21}R_{10}}e^{-\frac{4\Pi X_1 d_1}{\lambda}}\cos(\theta_{21}+\theta_{10}-\frac{4\Pi\nu_1 d_1}{\lambda})} \qquad [18]$$

Coefficients $R_{21}$ and $R_{10}$ are for the surface layer and substrate with bulk index values of $\nu_i$ and $\chi_i$ (equation [5]). Phase changes $\theta_{21}$ and $\theta_{10}$ due to reflection are calculated from equations similar to equation [6]. The total phase change, $\theta'$, between the incident and the total reflected waves includes changes due to reflection and to optical path differences (see equation [17]). Multiplying the numerator and denominator of equation [17] by the complex conjugate of the denominator and isolating the real and imaginary parts, we obtain the two following equations leading to values for $\theta'$:

$$\rho'\sin\theta' = \frac{\sqrt{R_{21}}(1-R_{10}e^{-\frac{8\Pi X_1 d_1}{\lambda}})\sin\theta_{21}+\sqrt{R_{10}}(1-R_{21})e^{-\frac{4\Pi X_1 d_1}{\lambda}}\sin(\theta_{10}-\frac{4\Pi\nu_1 d_1}{\lambda})}{1+R_{21}R_{10}e^{-\frac{8\Pi X_1 d_1}{\lambda}} + 2\sqrt{R_{21}R_{10}}e^{-\frac{4\Pi X_1 d_1}{\lambda}}\cos(\theta_{21}+\theta_{10}-\frac{4\Pi\nu_1 d_1}{\lambda})} \qquad [19]$$

and

$$\rho'\cos\theta' = \frac{\sqrt{R_{21}}(1+R_{10}e^{-\frac{8\Pi X_1 d_1}{\lambda}})\cos\theta_{21}+\sqrt{R_{10}}(1+R_{21})e^{-\frac{4\Pi X_1 d_1}{\lambda}}\cos(\theta_{10}-\frac{4\Pi\nu_1 d_1}{\lambda})}{1+R_{21}R_{10}e^{-\frac{8\Pi X_1 d_1}{\lambda}} + 2\sqrt{R_{21}R_{10}}e^{-\frac{4\Pi X_1 d_1}{\lambda}}\cos(\theta_{21}+\theta_{10}-\frac{4\Pi\nu_1 d_1}{\lambda})} \qquad [20]$$

Substituting the expression containing $\nu$ and $\chi$, for the layer and substrate, for $R_{21}$ and $R_{10}$ (equation [5]) leads to a rearrangement of equation [18] with a form very close to that reported by Tomlin (47).

Reflectance and transmission of a transparent substrate covered with multiple homogeneous layers has been discussed by Mouchart (31) (32). For **absorbing** compounds, equation [18] can easily be extended to a description of multiple thin absorbing layers superimposed on top of each other on the substrate.

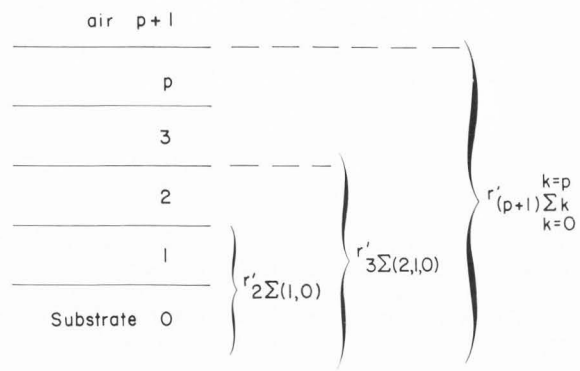


Fig. 3: Equivalent reflectance coefficient for the amplitude for a substrate covered with multiple superimposed homogeneous thin layers.

Let the substrate be labelled 0 and each successive layer labelled 1, 2, ...p + 1 where p + 1 is air as shown in Fig. 3. The substrate covered with a single layer may be considered from a reflectance point of view as a single equivalent substrate with a complex reflection coefficient of amplitude r' derived from equation [8]. For the following, the coefficient r' is renamed as $r'_{2\Sigma(1,0)}$ indicating that the coefficient is equivalent to that of the original material covered with a single layer placed in air. Assuming this equivalent substrate is again covered with a thin layer (2) and placed in air (3) the reflectance coefficient for two layers would be:

$$r'_{3,\Sigma(2,1,0)} = \frac{r_{32}+r'_{2,\Sigma(1,0)}e^{-j\varphi_2}}{1+r_{32}\,r_{2,\Sigma(1,0)}e^{-j\varphi_2}} \qquad [21]$$

By an iterative procedure we may calculate the reflectance coefficient for a substrate covered with p successive layers as the reflectance of a single layer, p, deposited on top of a substrate equivalent to the original substrate with p - 1 layers. The outer layer is in contact with the air and is labelled (p + 1). The resulting coefficient may then be expressed as follows:

$$r'_{(p+1)\Sigma p\cdots 0} = \frac{r_{(p+1)p}+r'_{p\Sigma p-1\cdots 0}e^{j\varphi_p}}{1+r_{(p+1)p}r'_{p\Sigma p-1\cdots 0}e^{-j\varphi_p}} = \rho'_{(p+1)\Sigma p\cdots 0}e^{-j\theta'_{(p+1)\Sigma p\cdots 0}} \qquad [22]$$

This relation allows one to calculate the resulting reflectance coefficient for intensity $R_{(p+1)\Sigma k}$ and the phase coefficient $\theta_{(p+1)\Sigma k}$ for a substrate covered with p layers and placed in the air :

$$R_{(p+1)\sum_0^p k} = \qquad [23]$$

$$\frac{R_{(p+1)p}+R'_{p\sum_0^{p-1}k}e^{-\frac{8\Pi X p d_p}{\lambda}} + 2\sqrt{R_{(p+1)p}R'_{p\sum_0^{p-1}k}}e^{-\frac{4\Pi X p d_p}{\lambda}}\cos(\theta_{(p+1)p}-\theta'_{p\sum_0^{p-1}k}+\frac{4\Pi\nu_p d_p}{\lambda})}{1+R_{(p+1)p}R'_{p\sum_0^{p-1}k}e^{-\frac{8\Pi X p d_p}{\lambda}} + 2\sqrt{R_{(p+1)p}R'_{p\sum_0^{p-1}k}}e^{-\frac{4\Pi X p d_p}{\lambda}}\cos(\theta_{(p+1)p}+\theta'_{p\sum_0^{p-1}k}-\frac{4\Pi\nu_p d_p}{\lambda})}$$

Fig. 4a

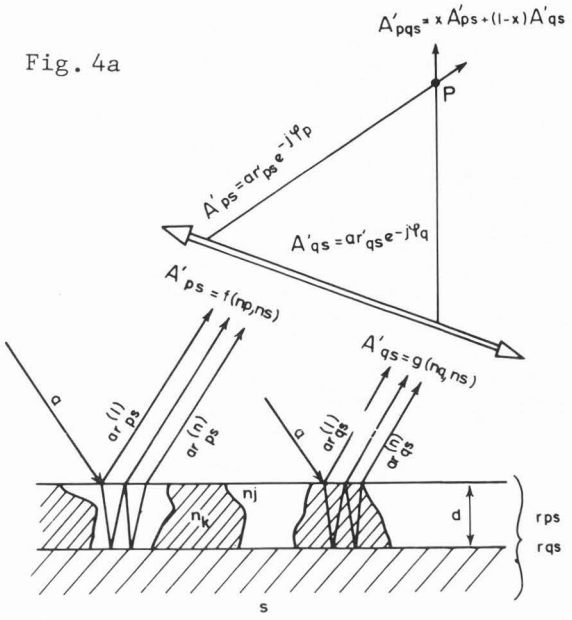


Fig. 4b

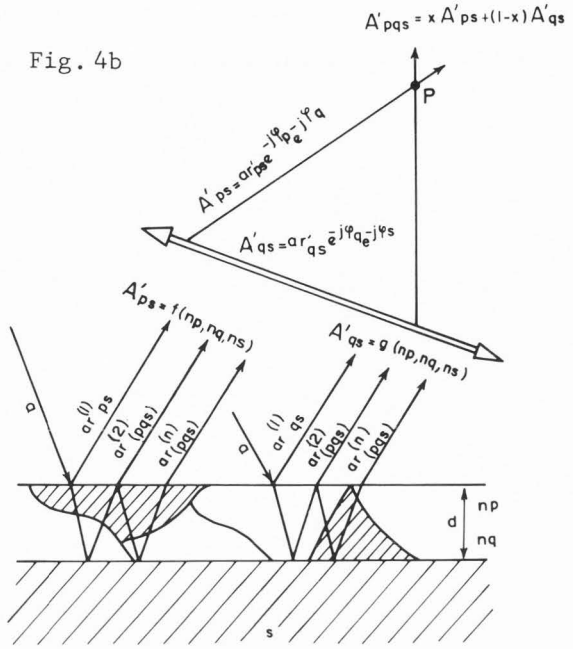


Fig. 4: Amplitudes of the emitted waves at the surface of a heterogeneous thin film consisting of p and q phases
a) phases act as independent particles, and
b) phases act as dependent particles.

---

and

$$\tan\theta_{(p+1)\sum_0^p k} = \frac{\sqrt{R_{(p+1)p}}(1-R'^{\,p-1}_{p\sum_0 k})\,e^{-\frac{8\Pi\chi pd_p}{\lambda}})\sin\theta_{(p+1)p} + \sqrt{R'^{\,p-1}_{p\sum_0 k}}(1-R_{(p+1)p})\,e^{-\frac{4\Pi\chi pd_p}{\lambda}}\sin(\theta'^{\,p-1}_{p\sum_0 k} - \frac{4\Pi\nu_p d_p}{\lambda})}{\sqrt{R_{(p+1)p}}(1+R'^{\,p-1}_{p\sum_0 k}\,e^{-\frac{8\Pi\chi pd_p}{\lambda}})\cos\theta_{(p+1)p} + \sqrt{R'^{\,p-1}_{p\sum_0 k}}(1+R_{(p+1)p})\,e^{-\frac{4\Pi\chi pd_p}{\lambda}}\cos(\theta'^{\,p-1}_{p\sum_0 k} - \frac{4\Pi\nu_p d_p}{\lambda})} \quad [24]$$

Equation [23] is directly derived from equations [19] and [20]. In equations [23] and [24] each R and θ parameter is calculated according to equations [5] and [6].

## Reflectance with a single heterogeneous surface layer

Assume that the thin surface layer consists of two distinct phases, p and q, on the substrate, s, that the layer is thin and that the dimension of the phases are small as compared to the wavelength of incident light. Assume also that each small particle can be characterized by the optical constants, ν and χ, of the bulk material. Within the illuminated area, each small particle will create reflected waves from both reflection and transmitted waves. Depending upon the spatial resolution and size, scattering from the two phases may be independent or dependent as illustrated in Figures 4a and 4b, respectively. If the particles act independently, then waves reflected from p never enter q and vice versa. Dependent behavior means the opposite. The reflectance for both cases will be discussed.

**Independent particles** (Figure 4a). Let the fraction of phases p and q be x and y, respectively (x + y = 1). If p and q are present on the surface of the substrate, s, then each binary system (p on top of s, and q on top of s) has a coefficient of reflection ($R'_{ps}$ or $R'_{qs}$ and phase coefficients $\theta'_{ps}$ or $\theta'_{qs}$). These coefficients are calculated from equations [14], [15] and [16]. Each system gives a reflected wave whose complex amplitude is $A'_{ps}$ and $A'_{qs}$ and the amplitude reaching the detector is :

$$A'_{pqs} = (xA'_{ps} + (1-x)\,A'_{qs}) = ar'_{pqs} = a\rho'_{pqs}e^{j\theta_{pqs}} \quad [25]$$

The measured intensity at the detector is:

$$I = A'_{pqs}\,A'^{*}_{pqs} = a^2R'_{pqs} \quad [26]$$

in which $R'_{pqs} = \rho'^2_{pqs}$ is the resulting reflectance coefficient given by:

$$R'_{pqs} = x^2R'_{ps} + (1-x)^2R'_{qs} + 2x(1-x)\sqrt{R'_{ps}R'_{qs}}\,\cos(\theta'_{ps} - \theta'_{qs}) \quad [27]$$

Based on equation [21] the resulting phase coefficient, $\theta'_{pqs}$ is:

$$\tan\theta'_{pqs} = \frac{x\sqrt{R'_{ps}}\sin\theta'_{ps} + (1-x)\sqrt{R'_{qs}}\sin\theta'_{qs}}{x\sqrt{R'_{ps}}\cos\theta'_{ps} + (1-x)\sqrt{R'_{qs}}\cos\theta'_{qs}} \quad [28]$$

Assuming the phases at the surface of the substrate are placed in contact with air, the coefficients $R'_{ps}$, $R'_{qs}$, $\theta_{ps}$ and $\theta'_{qs}$ may be directly calculated as a function of the ν and χ parameters of each phase from equations [14], [15] and [16], in which the index 2 refers to the air, the index 0 corresponds to the substrate, s, and the index 1 is set to p or q.

**Dependent particles** (Figure 4b). In this case the reflected waves from phases p or q interact with phase q or p respectively before emerging at the outer surface of the heterogeneous layer. The complex amplitude of each individual wave after reflection and transmission through the layer will depend on both phase changes $\theta_{ps}$ and $\theta_{qs}$. These phase changes take into account shifts due to interface reflection and path differences. As a result :

$$A'_{ps} = a\,\rho'_{ps}\,e^{j(\theta'_{ps}+k\theta'_{qs})} \qquad [29]$$

and

$$A'_{qs} = a\,\rho'_{qs}\,e^{j(\theta'_{qs}+k\theta'_{ps})} \qquad [30]$$

where k is the number of passes of the wave through the thin film. For p and q with volume fractions x and (1-x), respectively, the resulting amplitude is (as in equation [25]).

$$A'_{pqs} = \left[ x A'_{ps} + (1-x) A'_{qs} \right] = a\,r'_{pqs} \qquad [31]$$

In determining the reflected intensity, AA*, the phase $k\theta'_{qs}$ and $k'\theta'_{ps}$ will cancel due to random values of these phase differences. The total phase difference only depends upon $\theta'_{ps}$ and $\theta'_{qs}$ so that the situation is equivalent to the case of independent particles. The resulting reflectance coefficient is again given by equation [27] and the reflectivity of a heterogeneous surface is independent of the spatial distribution of the phases.

## Practical considerations

In order to calculate R and $\theta$ and therefore reflectance curves, values for $\nu$ and $\chi$ must be known over the range of wavelengths used for analysis. It is important to understand how the optical constants may be obtained and used for reflectance calculation, especially when the optical properties are anisotropic.

### Determination of $\nu$ and $\chi$

A variety of methods to determine $\nu$ and $\chi$ have been discussed (26). Minerals are commonly present as small inclusions in ores and rocks, so $\nu$ and $\chi$ are most often derived from microreflectometry measurements. The Koenigsberger method is often used for this purpose, and consists of solving two equations containing $\nu$ and $\chi$ for reflectance measured for normally incident light in air and oil successively (5), (16).

The optical constants, $\nu$ and $\chi$, may be derived from two reflectance measurements according to:

$$\nu = \frac{1}{2}\,\frac{N^2-1}{N\left(\frac{1+RH}{1-RH}\right)-\left(\frac{1+R}{1-R}\right)} \qquad [32]$$

$$\frac{\chi^2}{\nu^2} = \frac{2}{\nu}\left(\frac{1+R}{1-R}\right) - \frac{\nu^2+1}{\nu^2} \qquad [33]$$

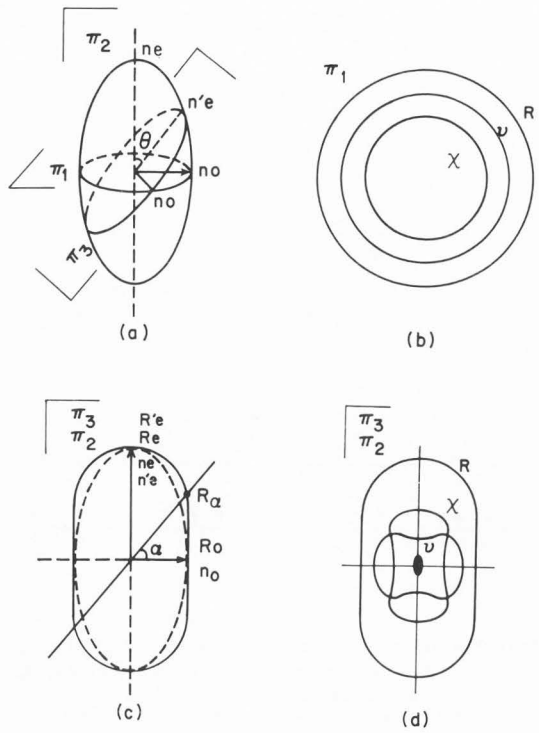


Fig. 5: Indicatrix surfaces for the refractive index and reflectance
a) uniaxial anisotropic crystal: refractive index ellipsoïd.
b) $\nu$, $\chi$, R for the isotropic plan.
c) refractive index and reflectance for a plan containing the optical axis
d) $\nu$, $\chi$, R for a plan containing the optical axis.

where R is the reflectance measured in air, $R_H$ is the reflectance measured for oil incident medium with refractive index N.

To be used in equations [32] and [33], R and $R_H$ measurements must satisfy the two following requirements.

(i) normally incident light relative to the normal direction of the specimen surface

(ii) the incident and reflected vibrations must remain linearly polarized with the same azimuth.

For cubic minerals, the optical symmetry is isotropic and the Koenigsberger equations may be solved for reflectance measurements from any surface independent of its orientation relative to the crystallographic directions. For uniaxial and biaxial anisotropic crystals, the situation is much more complex as discussed by Caye and Cervelle (6) and Cervelle et al. (13).

Crystals having hexagonal or tetragonal symmetry exhibit uniaxial anisotropy. Orthorhombic, triclinic and monoclinic crystals exhibit biaxial optical properties.

A schematic representation of the indicatrices in three dimensions of the refractive index (ellipsoïd) and reflectance (ovaloïd) for a positive uniaxial crystal ($n_e > n_o$) is shown in Fig. 5. The ellipsoïd and ovaloïd indicatrices for n and R respectively are coaxial (see reference (20) for a detailed discussion of optical properties related to their crystallographic structure). If the mineral were polished with the surface perpendicular to the optical axis (z axis in Fig. 5) the section of the ellipsoïd and ovaloïd are circles, thus, the refractive index and corresponding reflectance $n_o$ and $R_o$ will be independent of the azimuth of the incident vibration relative to the incident plane, containing both incident and reflected light beams. However, any surface containing the optical axis is characterized by two major and minor axes of the ellipse resulting from the intercept of the index ellipsoïd with the analyzed plane. The associated reflectances are $R_o$ and $R_e$ for a plane (linearly) - polarized vibration aligned along each of the two principal directions $n_o$ and $n_e$ respectively. A polished mineral surface usually represents a random orientation. For a surface orientated with an angle $\theta$, relative to the optical axis, the section of the refractive index ellipsoïd is still an ellipse. The two axes of the ellipse correspond to $n_o$ and $n'_e$ given by:

$$\frac{1}{n'_e} = \frac{\cos^2\theta}{n_o^2} + \frac{\sin^2\theta}{n_e^2} \qquad [34]$$

The minor axis of the ellipse represents $n_o$, and the major axis correspond to $n'_e$ where $n_o < n'_e \leq n_e$ for a negative uniaxial crystal. For a positive uniaxial crystal, the inequality signs are reversed. The associated reflectances are $R_o$ and $R'_e$ respectively. For any plane characterized by $n_o$ and $n'_e$ ( $R_o$, $R'_e$), any linearly polarized incident vibration with an angle $\alpha$ relative to the $n_o$ axis is decomposed into two vibrations aligned along the two principal directions respectively. The two reflected vibrations are recomposed and the corresponding reflectance, $R_\alpha$, is given by:

$$R_\alpha = R_o \sin^2\alpha + R'_e \cos^2\alpha \qquad [35]$$

The $\alpha$ ranging from 0 to 360°, equation [35] represents the indicatrix surface of the reflectance for the analysed surface.

For complex refractive indices, the $\nu$ and $\chi$ ellipsoïds and the R ovaloïd are coaxial volumes. Their axes are those of the crystallographic axes of symmetry of the crystal.

For a linearly polarized incident vibration aligned along one of the two principal directions ($n_o$, $n_e$) or ($n_o$, $n'_e$) the reflected light will remain linearly polarized in the same azimuth relative to the incident vibration. Thus, for any arbitrary surface plane of a uniaxial crystal, the polished specimen can be rotated to determine a maximum reflectance. by turning the sample 90°, the value of the minimum reflectance is determined. The Koenigsberger method may be applied to the reflectance measurements carried out in air and oil successively to determine the two sets ($\nu_o$, $\chi_o$) and ($\nu_e$, $\chi_e$).

For biaxial crystals, three sets of constants ($n_g$, $n_m$, $n_p$) are applicable. For crystals having an orthorhombic crystallographic symmetry, the Koenigsberger equations can be solved when the plane contains two principal directions allowing determination of two of the three constants, ($n_p$, $n_m$), ($n_g$, $n_p$) or ($n_g$, $n_m$) respectively. Therefore, for orthorhombic crystals the optical constants can be derived from reflectance measurements for surfaces containing principal optical directions. Moreover, a surface perpendicular to an optical axis is an isotropic surface characterized by the intermediate index value, $n_m$, and its associated reflectance, $R_m$. It is difficult to reduce reflectance data down to simple expressions for $\nu$ and $\chi$ of an arbitrarily orientated surface. Therefore, the Koenigsberger method does not apply for triclinic or monoclinic crystals (not used in this study).

## Comparison between Experimental and Calculated Reflectances Curves

The aim of comparing experimental to calculated reflectance curves is to identify the nature of an unknown mineral. As a result, many reference reflectance curves measured with normally incident light have been published by the International Mineralogical Association (IMA), Commission for Ore Microscopy, for both air and oil incident media. It is therefore convenient to simply compare data from bulk samples to these reference curves. The optical constants, $\nu$ and $\chi$, derived from the reference reflectance curves will be used in reflectance calculations by means of equations [5] [15] [22] and [27]. These reference reflectance data must satisfy the experimental conditions mentioned above, i.e., normally incident light, and linearly incident and reflected polarized light with the same azimuth and specimens with a known crystallographic orientation. For randomly orientated substrate and surface layers, reflectance curves may be used only on a qualitative basis by comparing experimental and calculated reflectance data. However, to be consistent with the reflectance calculations requirements, the experimental reflectance data must be obtained under normally incident illumination.

It will be shown that surface layers on bulk minerals can modify the reflectance curves, therefore it is necessary to consider the effects of anisotropy in both the layer and the substrate upon measured and calculated reflectance properties. The crystallographic orientation of the layer and the substrate are generally unknown (randomly orientated polished crystals) while the orientations of the crystals used for the reference data are known. It is important then to consider the limits defined by known orientation upon reflectance from unknown orientations. The limits are defined in Table 2 which shows that the calculated reflectance for isotropic films on isotropic substrate can be directly compared to experimental data (single set $\nu_o^S$, $\chi_o^S$ values for any randomly polished substrate and a single set $\nu_o^L$, $\chi_o^L$ of values for the surface film). For either a uniaxial layer on an isotropic substrate or vice versa the situation is more complicated. For an anisotropic compound having its optical axis perpendicular to the surface, the situation is equivalent to isotropic film and substrate and the experimental data are directly

comparable to calculated data. Thus, $\nu_o$ and $\chi_o$ values for the isotropic surface of the uniaxial film or substrate are used for calculations. For a surface containing the optical axis, the measured reflectance coefficients are $R_o$ and $R_e$ when the incident vibration is aligned along each of the two principal directions of the surface successively. Therefore two experimental reflectance curves must be measured successively. The first measurement corresponds to a position of the specimen leading to a maximum of reflectivity, the second measurement is obtained after rotating the specimen by 90°. Each experimental reflectance curve may be compared to calculated curves by using one of the two sets ($\nu_o$, $\chi_o$) and ($\nu_e$, $\chi_e$) successively. As discussed above, for an arbitrarily orientated surface, the reflectance coefficients measured along the two principal directions are $R_o$ and $R'_e$ respectively with $R'_e < R_o$. Since the angle between the surface and the optical axis of the anisotropic compound in the layer substrate assembly is unknown, the use of $\nu_e$ and $\chi_e$ data leads to a calculated reflectance which the upper limit of reflectivity to be compared to the $R'_e$ experimental curve.

As a result, for an anisotropic surface film on an isotropic substrate, the measured and calculated reflectance curves can only be compared by considering separately the two extreme values for the maximum and minimum reflectance curves measured along the two perpendicular principal directions of the surface successively. A similar situation is found for an isotropic layer on a uniaxial substrate. In practice, an average reflectance curve $\bar{R}$ may be obtained from a single measurement with the sample positioned midway between the orientation relative to the incident plan for maximum and minimum of reflectivity. For normally incident polarized light, the average curve of any randomly orientated surface of the uniaxial film on the isotropic substrate (and vice versa) will be $\bar{R} = R_o + R'_e / 2$. For comparison an average calculated reflectance curve, $\bar{R}$calc may be obtained by averaging the calculated curves considering the ($\nu_o$, $\chi_o$) and ($\nu_e$, $\chi_e$) optical constants of the uniaxial compound successively. Therefore the average calculated curve $\bar{R}calc = R(\nu_o, \chi_o) + R(\nu_e, \chi_e) / 2$ indicates an upper limit of the reflectance curve to be compared to the average experimental curve. The lower limit for the reflectance curve corresponds to the measured $R_o$, or calculated reflectance $R(\nu_o, \chi_o)$ for a surface perpendicular to the optical axis of the uniaxial crystal.

For a uniaxial layer on a uniaxial substrate, the reflectance extremes are dominated by either the layer or substrate anisotropy. Since the amount of transmitted light is $I_t = I_o \exp(-4\pi\chi d / \lambda)$ where $I_o$ is the incident intensity, when the layer is thick relative to absorption of light (i.e., $\chi d >> \lambda/4\pi$) then the layer dominates reflectance.

If the layer is thin (i.e., $\chi d << \lambda/4\pi$) then the substrate dominates the reflectance. In the following, for a weakly anisotropic substrate, such as chalcopyrite ($CuFeS_2$), the reflectance differences due to crystallographic orientation will depend mainly on the anisotropy of the surface layer.

For a biaxial surface layer on top of an isotropic substrate or vice versa, the same situation as discussed above must be considered by using for reflectance calculations each of the three sets of data ($n_p$, $n_m$), ($n_m$, $n_g$) and ($n_g$, $n_p$), successively. Association of uniaxial and biaxial compounds on top of each other will not be considered.

Thus, for uniaxial or biaxial layers on a substrate, comparisons between experimental and calculated reflectance curves will provide only qualitative information indicating the most probable surface compound among various minerals of similar qualitative composition with different crystallographic properties. In practice, extreme reflectance curves will be calculated by substituing extreme $\nu$ and $\chi$ values (principal optical directions of the layer and substrate compounds) in the previous equations [18] [23] and [27]. Thus, the experimental curves will be compared to the extreme situations shown in Table 2.

Table 2 - Comparisons between experimental and calculated reflectance curves

| Optical properties | | Resulting reflectance |
|---|---|---|
| Substrate | Surface layer | d : thickness<br>$R_m$: measured reflectance<br>$R^c$: calculated reflectance |
| Isotropic<br>$R^s_o$ | Isotropic<br>$R^L_o$ | $R_m = R^c_o$ |
| Isotropic<br>$R^s_o$ | Uniaxial anisotropy<br>$R^L_o$<br>$R^L_{e'} = \frac{R^L_o + R^L_e}{2}$ | $R_m = R^c_o$<br>and<br>$R^c_o \lesssim R_m \lesssim R^c_1$ |
| Uniaxial anisotropy<br>$R^s_o$<br>$R^s_{e'} = \frac{R^s_o + R^s_e}{2}$ | Isotropic<br>$R^L_o$ | $R_m = R^c_o$<br>and<br>$R^c_o \lesssim R_m \lesssim R^c_2$ |
| Uniaxial anisotropy<br>$R^s_o$<br>$R^s_{e'} = \frac{R^s_o + R^s_o}{2}$ | Uniaxial anisotropy<br>$R^L_o$<br>$R^L_{e'} = \frac{R^L_o + R^L_e}{2}$ | Case 1 $d\chi >> \lambda/4\pi$<br>$R_m = R^c_2$<br>and<br>$R^c_3 < R_m < R^c_4$<br>---<br>Case 2 $d\chi << \lambda/4\pi$<br>$R_m = R^c_2$<br>and<br>$R_o < R_m < R^c_1$ |

$R^c_o = [R^c (R^s_{o'}, R^L_{o'}, d)]$,

$R^c_1 = 1/2 [R^c (R^s_{o'}, R^L_{o'}, d) + R^c (R^s_{o'}, R^L_{e'}, d)]$

$R^e_2 = 1/2 [R^c (R^s_{o'}, R^L_{o'}, d) + R^c (R^s_{e'}, R^L_{o'}, d)]$,

$R^c_3 = R^c (R^L_{o'}, d)$ $\quad R^c_4 = 1/2 [R^c (R^L_{o'}, d) + R^c (R^L_{e'}, d)]$

## Effect of surface films on reflectance: Polished Chalcopyrite ($CuFeS_2$)

### Specimen preparation and reflectance measurements

The effects of polishing chalcopyrite crystals with diamond or chromic oxide abrasives has been reported previously (25) (41). Therefore, results will only be briefly reviewed before comparing experimental data to the reflectance curves calculated using the above procedures.

The specimens were bulk chalcopyrite originating from Le Burc deposit (Tarn. France). The samples were polished with diamond abrasives dispersed in silicone oil on an aluminum foil. Suspension of 6, 3, 1 and 0.5 μm particles were successively used. For each abrasive size the polishing time was one hour. For some samples, the polished surface was subsequently polished with distilled water and chromic oxide (0.25 μm) on a soft polishing cloth.

X-ray photoelectron (XPS) and Auger electron spectroscopy (AES) were used to study the surface composition of diamond and chromic oxide polished specimens, respectively (25) (41). A silicon and carbon rich surface layer was detected on diamond polished specimens resulting from the silicone oil used to disperse the diamond powder. Under the outer silicone contamination layer, the presence of sulfate, thin iron oxide, and thin Cu-rich sulfide chemical compounds were detected over the $CuFeS_2$ substrate. Only iron was bound in the sulfate. The iron oxide and sulfate layers were very thin since Fe, Cu and S belonging to the sulfide substrate were also simultaneously detected. This fact made it difficult to accurately identify the nature of all surface compounds due to overlap between the various Fe photoelectron peaks. For example, the chemically shifted Fe peak for $Fe_3O_4$ (magnetite) overlaps the Fe peak for $CuFeS_2$, and the Fe peak from $Fe_2O_3$ (hematite) or FeO.OH (goethite) overlaps the Fe peak from iron sulfate. The presence of iron oxide and iron sulfate were qualitatively shown but the nature of the compounds were not positively identified. A similar situation was encountered in the case of Cu-rich surface compounds. The chemical shift of Cu in an oxide versus sulfide is too small to separate. AES profiling data clearly show however, that copper is rejected from the surface to form a copper-rich layer under the sulfate/iron oxide layers (41). Both this copper-rich sulfide region and the XPS surface data were consistent with the Cu-rich sulfides, but the chemical shift was too small to distinguish between the presence of bornite ($Cu_5FeS_4$), covellite (CuS), or chalcocite ($Cu_2S$) under the iron oxide layer. We shall see that reflectance curves can supplement XPS data for chemical compound identification and can be used to narrow the possible compounds actually present on the surface.

In the case of a chromic oxide polished surface, the iron sulfate was not detected, presumably due to dissolution by water and/or mechanical removal by the chromic oxide polishing. A thinner iron oxide layer was still detected. Adsorbed water or hydroxy species were also detected by XPS as indicated by the shape of the oxygen photoelectron peak.

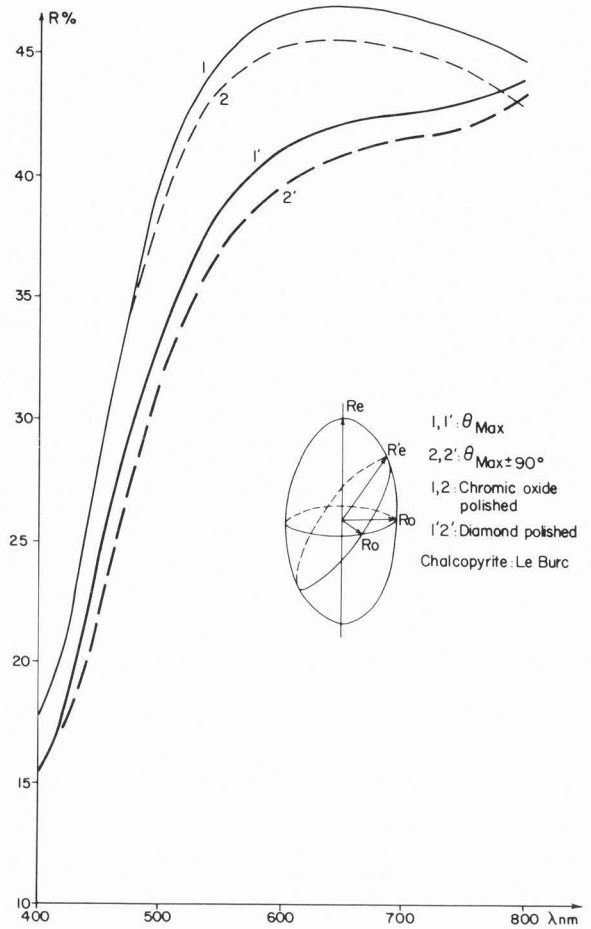


Fig. 6: Experimental reflectance curves for a diamond polished chalcopyrite (1',2') and a chromic oxide polished chalcopyrite (1,2). Measurements were carried out with normally incident polarized light with the sample rotated for a maximum reflectance (R'e) then rotated 90° for a minimum reflectance (Ro).

To determine the influence of these surface layers on the optical properties, the reflectance curves were measured with normally incident light between 400nm and 800nm using equipment described previously (5). The incident wavelength was increased in steps of 20nm. The analyzed area was ≃ 10μm in diameter. A SiC specimen was used as a reflectance standard. Since the reflectance curves will be calculated using equations [18], [23] and [27] derived for **normally incident light,** the present experimental data were taken through a 16x objective lens on the microscope with a numerical aperture of 0.4. This aperture results in a maximum deviation from normal incidence of ± 5°. The effects of this deviation could be corrected since the reflectance. $R_{i=o}$ for normal incidence is equal to $R_\theta^\perp + R_\theta'' / 2$ where $R_\theta^\perp$ and $R_\theta''$ are the reflection coefficients for light polarized perpendicular and parallel to the incidence plan respectively, and the light

is incident at an angle $\theta$ relative to the surface normal (valid for $\theta < 25°$). In general, our 5° deviation represents a negligible correction. In order to have a single measurement we used an illuminator equipped with a Berek (3 reflections) type prism and a polarizer providing a linearly polarized incident light at 45° relative to the incident plane (5). Moreover, for specimens exhibiting anisotropy, the sample was positioned midway between the orientations for maximum and minimum reflectance successively (see Table 2) (equivalent to a measurement with natural light for any azimuth relative to the specimen surface).

Chalcopyrite is a tetragonal crystal (uniaxial) exhibiting a weak anisotropy. The polished chalcopyrite specimen was placed on the specimen stage of the microscope, then rotated under the incident light beam until the measured reflected intensity exhibited a maximum. For this purpose, the wavelength was set at 580 nm corresponding to the maximum sensitivity of the detector, high intensity from the light source and high reflectance from $CuFeS_2$. The reflectance curve was measured from 400 to 800 nm for this position. The specimen was then rotated by an angle of 90° and the measurements repeated. Reflectance curves are given in Fig. 6 for diamond and chromic oxide polished surfaces. Diamond polished surfaces are characterized by a lower reflectivity than for chromic oxide polished specimens. For both diamond and chromic oxide polished $CuFeS_2$ specimens, there is a relatively small difference between the measured $R_o$ and $R'_e$ reflectance curves. These variations are much lower than the difference resulting from the polishing procedure.

## Calculated reflectance curves based on surface composition data

**Choice of $\nu$ and $\chi$ values used for calculation.** The optical parameters of the surface absorbing layers and of the substrate were derived from the reference reflectance data for minerals measured in air and in oil respectively as published by the International Mineralogical Association (IMA), Commission on Ore Microscopy (7-12) (44). However since determination of $\nu$ and $\chi$ required a polished section, the data will be affected by the surface chemical compounds created by polishing. To minimize these effects, optical constants for bulk chalcopyrite were taken from reflectance measurements (8) on a chromic oxide polished specimen since the surface chemical modification was least by this procedure. The reflectance curves for diamond polished specimens were then calculated accounting for the various chemical compounds where the layer thicknesses were approximated from surface analysis data. It was assumed that the surface compounds had optical properties equal to those of natural minerals of similar compositions.

Silicon/carbon compounds and iron sulfate were found on the surface of diamond polished chalcopyrite. The Si and C contamination layer was considered to be a transparent material ($\chi = 0$) having an index, $\nu$, equal to 1.52 at 589 nm (equivalent to that of a silicone oil). Iron sulfate has also been considered to be a transparent material, but the value of $\nu$ at 589 nm varies from 1.48 for $FeSO_4.H_2O$ to 1.82 for $Fe_2.(SO_4)_3$. The values of $\nu$ at other wavelengths were approximated by assuming a normal distribution curve similar to that of quartz.

The chalcopyrite substrate is weakly anisotropic as shown in Fig. 6. Therefore, the $\nu_o$ and $\chi_o$ indices of the isotropic plan is used for calculation in the present study. Magnetite ($Fe_3O_4$), bornite ($Cu_5FeS_4$) and wustite (FeO) are isotropic materials characterized by a single set of $\nu$ and $\chi$ data derived from reference reflectance data (9) (7) (10) using the Koenigsberger equations. Hematite ($Fe_2O_3$) and Covellite (CuS) have uniaxial optical anisotropy. Two sets of optical constants were derived from reflectance data from the literature (12) (14). Goethite (FeO.OH) and chalcocite ($Cu_2S$) are orthorhombic crystals exhibiting a biaxial anisotropy. For the goethite, reflectance data from the literature were used, but the surface had an unknown crystallographic orientation (11). The values of $\nu$ calculated from ref. (11) are consistent with those reported for (Na), i.e. : 2.26, 2.393 and 2.398 for $\nu_p$, $\nu_m$, $\nu_g$ respectively. Since the values of the indices are very close, we can assume that the optical constant derived from the reflectance measurements (11) are the extreme sets of values ($\nu_p$, $\chi_p$) and ($\nu_g$, $\chi_g$).

For the chalcocite ($Cu_2S$) reflectance measurements in air and oil were measured for three differents orientations (45). The reflectances differ less than 1 %. Thus, only the intermediate constants ($\nu_m$, $\chi_m$) were used in the reflectance calculations.

**Calculated reflectance curves.** Reflectance curves were calculated for chalcopyrite covered by single layers from 1 to 20 nm thick. Transparent compound surface layers of $Fe_2(SO_4)_3$, $FeSO_4.5H_2O$, or silicone oil only slightly decreased the percent reflectance as compared to reference data. Even if the layer was an absorbing compound, the percent reflectance decreased but the shape remained similar to that of the reference curve for thicknesses less than 10 nm. Above 10 nm, absorbing layers normally led to a minimum in the reflectance curve as shown in Fig. 7a for a single layer of FeO.OH, $Fe_2O_3$ or $Fe_3O_4$. For a single homogeneous iron oxide layer, 20 nm thick FeO.OH or $Fe_3O_4$ similarly led to a low minimum (5 %) in reflectivity at wavelengths $\geq$ 460 nm (Fig. 7b). For an $Fe_2O_3$ layer, a minimum was detectable for thickness $\geq$ 10 nm but the reflectance value was larger than for FeO.OH or $Fe_3O_4$ layers. For all absorbing layers, the wavelength of the minimum reflectance moved towards longer wavelengths as the thickness of the layer was increased (Fig. 7c).

Electron spectroscopy showed that both iron oxide and copper rich sulfide were simultaneously present at the surface of the diamond polished chalcopyrite. The analytical procedure used did not allow us to resolve the spatial organization of these compounds. Reflectance curves were therefore calculated considering both superimposed homogeneous layers and a single heterogeneous layer. In order to simplify calculations only $Fe_3O_4$ - $Cu_5FeS_4$ binary compounds will be presented since the results are representative.

For two homogeneous layers, the thickness of each layer was varied so that the total thickness was either 10 or 30 nm (equation [23]). These calculations were compared to reflectance curves calculated assuming a single heterogeneous layer in which the volume fraction of the compounds had the same proportion as layer thicknesses in homogeneous layers. Calculated curves are shown in Fig. 8 for a single heterogeneous $Fe_3O_4/Cu_5FeS_4$ layer with thicknesses of 10 or 30 nm. For a total thickness of less than 10 nm

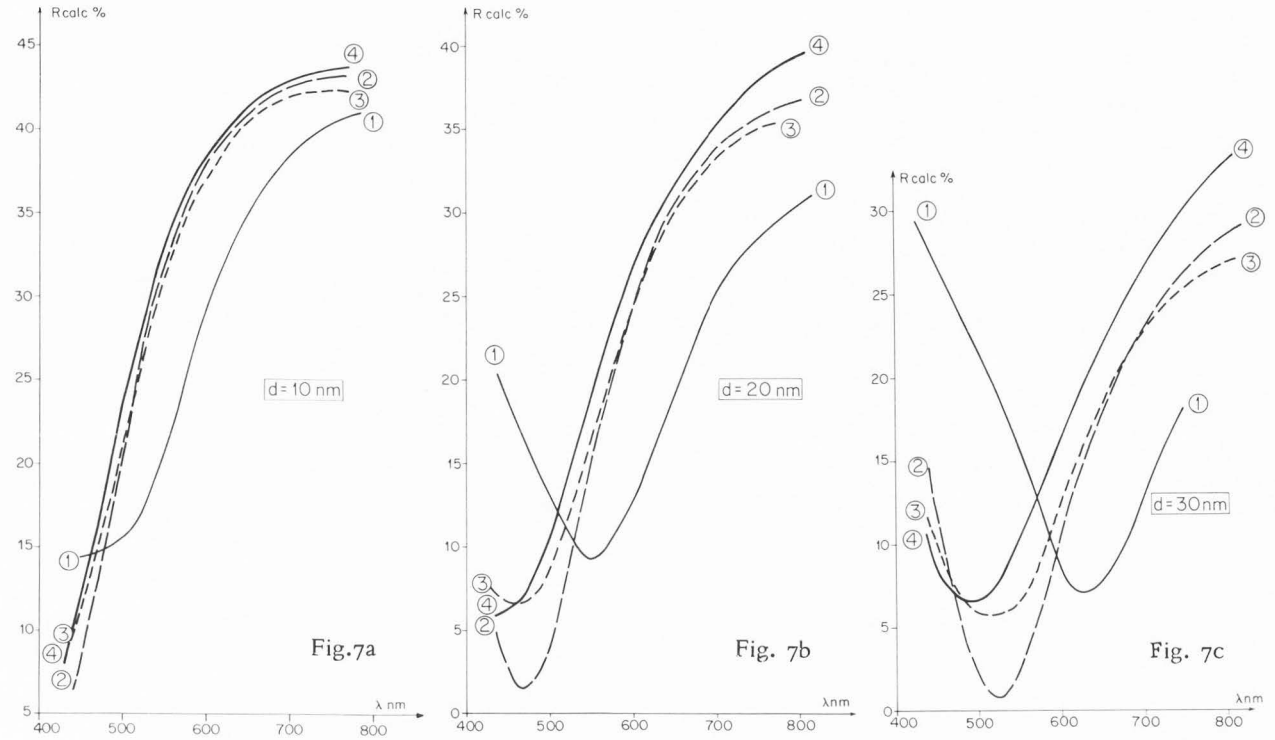


Fig. 7: Calculated reflectance curves for chalcopyrite covered with a single homogeneous layer of $Fe_2O_3$ (1), FeO.OH (2), $Fe_3O_4$ (3) and FeO (4) with thickness of 10 nm (a), 20 nm (b) and 30 nm (c) successively.

the difference between the reflectance for two homogeneous or one heterogeneous layer was less than 1.5 % (Table 3).

This difference increased when the thickness of the layer was increased and became greater than the experimental error ($\pm$ 2 %) for d > 10 nm. If other compounds were considered, the results were similar. For FeO.OH/$Cu_5FeS_4$ compounds 10 nm thick the relative difference between homogeneous layers and a heterogeneous layer was less than for $Fe_2O_3/Cu_5FeS_4$ compounds, but homogeneous vs. heterogeneous must still be considered for surface layers > 10 nm thick. Since surface analysis suggested the layer thicknesses on $CuFeS_2$ were $\leq$ 10 nm, the influence of other parameters upon the calculated curves will be examined independent of the heterogeneous or homogeneous models.

By equation [18], the exponential term and in turn the resulting reflectance is linearly dependent on thickness for layer thicknesses $\leq$ 30 nm. Since the reflectance is a summation over all layers, variations in the thickness of oxide versus sulfide layers at a constant total thickness also results in a second linear variation of reflectance. This is illustrated in Fig. 9 for superimposed layers of $Fe_3O_4$ on top of $Cu_5FeS_4$ with thickness $d_1$ and $d_2$, respectively. The sum $d_1 + d_2$ was constant at 10 nm and reflectance at different wavelengths is plotted as a function of the percent of $Fe_3O_4$ in the total thickness. Note that even though linear variations are observed at each wavelength, the reflectance curves change shape since the slope is a function of wavelengths.

For heterogeneous layers where the oxide and sulfide are intermixed in a single thin layer, the effect of variations in volume fraction at a constant thickness (10 nm) are similar to those for the two superimposed homogeneous layers model. The reflectance has been shown to vary linearly with the fraction of iron oxide in a layer (x) containing a fraction (1-x) of copper sulfide. Linear dependence of the calculated reflectance versus the proportion x and (1-x) of the two surface compounds will be illustrated below.

In order to show the dependence of the reflectance upon the nature of the iron oxide and the copper-rich sulfide on a chalcopyrite substrate, curves were calculated by varying the nature of both the iron oxide (outer layer) of the copper sulfide (intermediate layer). Calculations were carried out for a 15 nm outer iron oxide layer and a 5 nm thick $Cu_2S$ or $Cu_5FeS_4$ intermediate layer. Results in Fig. 10a and Fig. 10b show the reflectance curves consist of two groups differentiated by the nature of the iron oxide (independent of the intermediate copper sulfide layer). An $Fe_2O_3$ layer over the copper sulfide always led to higher reflectance values between 400 to 520 nm when compared to outer layers of $Fe_3O_4$ or FeO.OH. For wavelengths greater than 520 nm the shape of the curves remain within a few percent of one another.

By increasing the thicknesses of the iron oxide and the copper sulfide layers simultaneously, again two groups of curves are obtained when $Fe_2O_3$ is compared

Table 3 - Percentage difference ($R_{HO}$ - $R_{HE}$) between calculated reflectance values assuming the surface binary $Fe_3O_4/Cu_5FeS_4$ compounds exist as in:
- two superimposed single layers of thickness $d_1$ and $d_2$ respectively leading to a fraction $x = d_1 / d_1 + d_2$ of $Fe_3O_4$ ($R_{HO}$)
- a single heterogeneous layer of thickness ($d = d_1 + d_2$) containing a volume fraction, x, of $Fe_3O_4$ ($R_{HE}$)

**Thickness of the surface layer(s): 10 nm**

| λ nm | fraction of $Fe_3O_4$ in the binary compound $Fe_3O_4/Cu_5FeS_4$ 0.2 | 0.4 | 0.6 | 0.8 |
|---|---|---|---|---|
| 440 | 1 | 1.4 | 1.5 | 0.1 |
| 480 | 0.4 | 0.7 | 0.8 | 0.5 |
| 520 | 0 | 0.1 | 0.1 | 0.1 |
| 560 | 0.2 | 0.2 | 0.2 | 0.2 |
| 600 | 0.24 | 0.3 | 0.3 | 0.2 |
| 640 | 0.25 | 0.4 | 0.3 | 0.2 |
| 700 | 0.35 | 0.5 | 0.5 | 0.3 |

**Thickness of the surface layer(s): 30 nm**

| λ nm | fraction of $Fe_3O_4$ in the binary compound $Fe_3O_4/Cu_5FeS_4$ 0.2 | 0.4 | 0.6 | 0.8 |
|---|---|---|---|---|
| 440 | 0.6 | 0.6 | 1.6 | 1.6 |
| 480 | 13.5 | 21.6 | 19.8 | 10.6 |
| 520 | 7.86 | 16.5 | 21.5 | 16.2 |
| 560 | 2.1 | 5.7 | 8.9 | 8.3 |
| 600 | 0.1 | 1.3 | 3.1 | 3.5 |
| 640 | 1.0 | 0.8 | 0.2 | 1.0 |
| 700 | 2.5 | 3.5 | 3.0 | 1.6 |

Fig. 8: Calculated reflectance curves for chalcopyrite covered with a 10 nm and 30 nm thick single heterogeneous layer consisting of $Fe_3O_4$ in volume fraction, x, and $Cu_5FeS_4$ in volume fraction (1-x) respectively.

Fig. 9: Linear dependence of the calculated reflectance for selected wavelengths as a function of the percent thickness of two superimposed homogeneous films on top of a chalcopyrite specimen. The outer $Fe_3O_4$ and the inner $Cu_5FeS_4$ have thickness $d_1$ and $d_2$ respectively such as $d_1 + d_2 = 10$ nm.

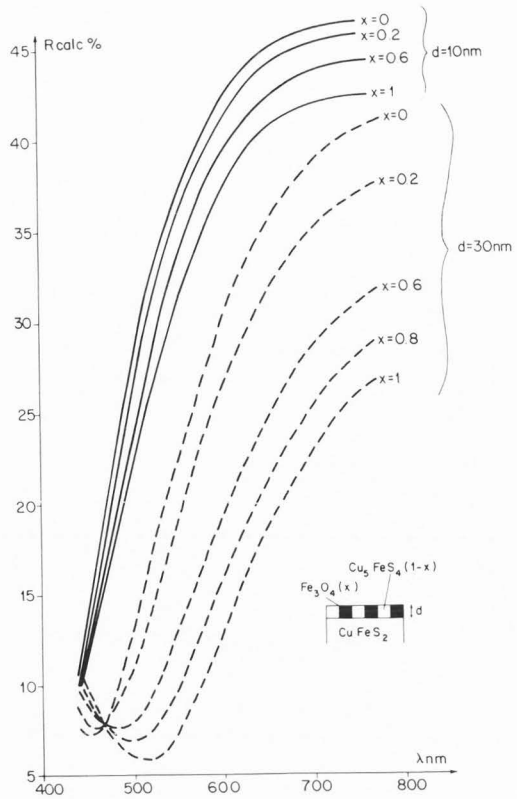


Fig. 8

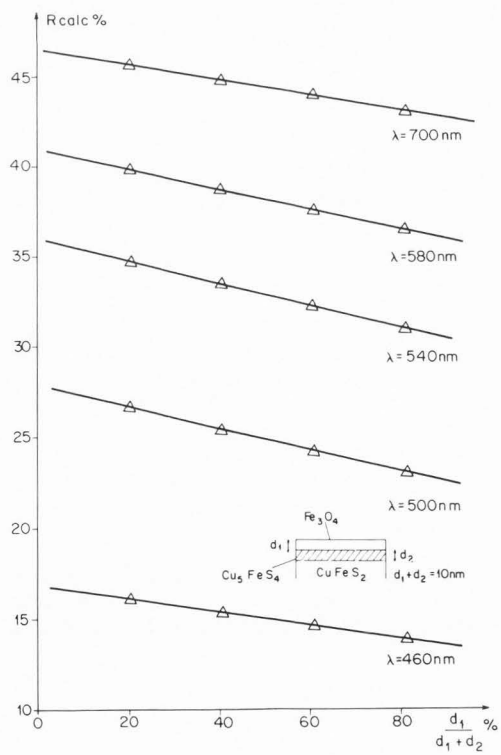


Fig. 9

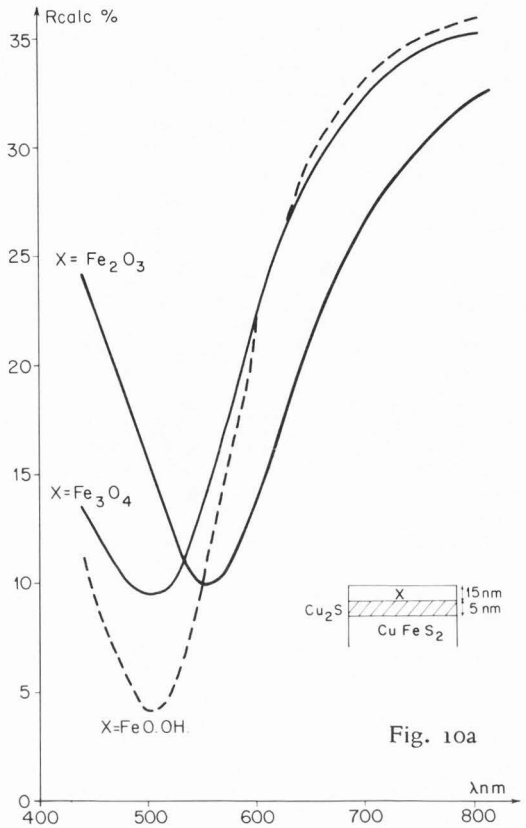


Fig. 10a

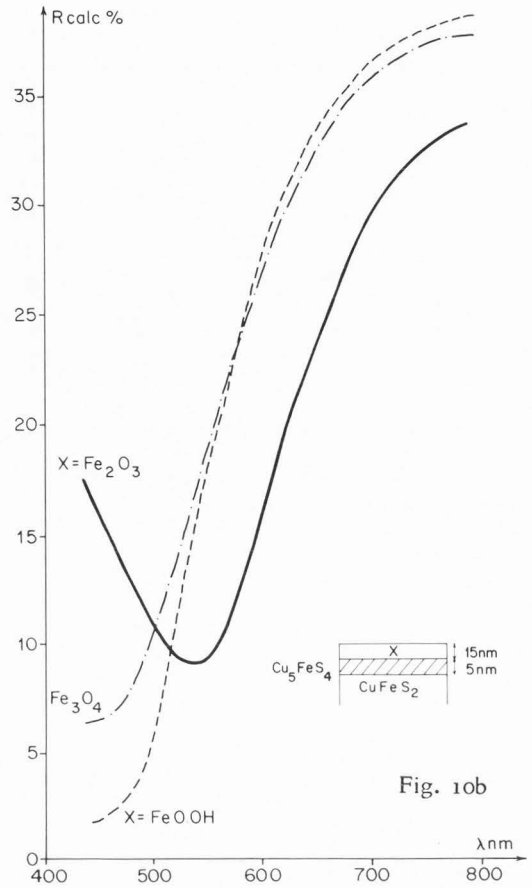


Fig. 10b

Fig. 10: Calculated reflectance curves for chalcopyrite covered with homogeneous bilayers of $Fe_2O_3$, $Fe_3O_4$ and FeO.OH outer layer on top of $Cu_2S$ intermediate layer (a) or on top of a $Cu_5FeS_4$ intermediate layer (b). The thicknesses of the outer iron oxide layer and copper rich intermediate layer are 15 and 5 nm respectively.

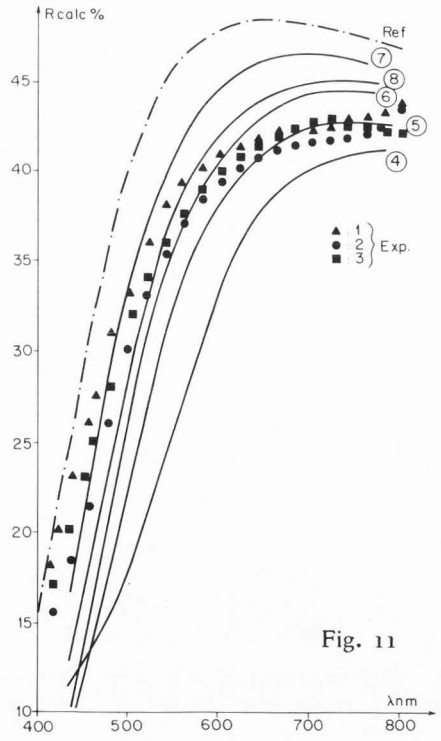


Fig. 11

Fig. 11: Comparisons between experimental and calculated reflectance curves. **Experimental curves:** (1), (2), (3), (Ref.), experimental curves for measurements carried out a few hours (1), a few days after polishing the specimen (2) (3) experimental curve for a second specimen separately polished and (Ref.) experimental reference reflectance curve from reference (8)
**Calculated curves:** (4), (5), (6), (7), (8) calculated reflectance curves for
(4) 5 nm $Fe_2O_3$ on top of 5 nm $Fe_3O_4$.
(5) 5 nm FeO on top of 5 nm $Fe_3O_4$
(6) 5 nm $Fe_3O_4$ on top of 5 nm $Cu_5FeS_4$
(7) 2.5 nm $Fe_3O_4$ on top of 5 nm $Cu_5FeS_4$
(8) 5 nm $Fe_3O_4$ on top of 2.5 nm $Cu_5FeS_4$ .

to $Fe_3O_4$ or FeO.OH. A layer of $Fe_2O_3$ always leads to higher reflectivity and a reflectance minimum at longer wavelengths than for $Fe_3O_4$ or FeO.OH. For all iron oxide outer layers, the absolute reflectance and minima values also depend on the type of the intermediate copper rich sulfide layer.

**Diamond versus chromic oxide polished chalcopyrite surfaces.** The reflectance curve has been calculated assuming the reference surface (derived from experimental data of chromic oxide polished chalcopyrite) to be successively or simultaneously covered by transparent materials (silicone oil and iron sulfate) and absorbing materials (iron oxide and copper rich sulfide). For a total thickness of all layers ranging from 1 to 10 nm the calculated reflectance was independent of assuming homogeneous layers or a heterogeneous layer.

The presence of surface layers of iron oxide and copper rich sulfide are particularly effective in modifying the shape and magnitude of the reflectance curve. Electron spectroscopy data showed the types of surface layers and approximate thickness (10 nm). Although the data suggested homogeneous layers, it was not sufficient to absolutely distinguish between iron oxide and copper sulfide distributed heterogeneously versus homogeneously. Reflectance calculation showed that the shape of the reflectance curves will be dependent upon the geometrical arrangement for thicknesses $\geq$ 20 nm. It is difficult to achieve an accurate measurement of the thickness of the oxidized layer either from ESCA and AES depth profiling or from comparisons between experimental and calculated reflectance curves. Moreover, the surface composition changes probably result from temperature increases during polishing. While the thickness of the oxidized layer may depend upon the time of polishing, the quantity of liquid used as a carrier of the abrasives, the load applied, and the length of time between polishing and reflectance measurements. The data in Fig. 11 show that our polishing procedures were reproducible. Two pieces of chalcopyrite originating from the same deposit were separately diamond polished. Curves # 1 and # 2 in Fig. 11 correspond to the same specimen measured a few hours (# 1) and a few days after polishing (# 2). Curve # 3 corresponds to the second piece of chalcopyrite which was polished separately with the same experimental condition. The differences between curves # 1 and # 3 are very small.

The surface analysis data indicate that the surface layers have a thickness less than 10 nm. The calculated and experimental reflectance curves agree when 7.5 nm heterogeneous surface compound is assumed to contain $Fe_3O_4$ and $Cu_5FeS_4$ with fractions of 0.7 and 0.3 respectively. Obviously, this is not a unique solution since small changes in the values of the fraction, x, and the thickness, d, and reciprocally will lead to consistency between experimental and calculated curves. Similarly, $Fe_3O_4$ and $Cu_5FeS_4$ in the layer is not a unique solution since different iron oxides and copper sulfides can be assumed to be present and yield an equally good agreement to experimental data when the thickness is allowed to vary but remain below 10 nm. It is obvious though that thin surface layers (< 10 nm) strongly modify the reflectance properties of chalcopyrite.

## Sensitivity of optical microreflectometry and microscopy to surface layers and changes in their thicknesses

### Hue and luminosity

For a monochromatic incident light beam with wavelength, $\lambda$, the measured reflected intensity, $I_R$, is :

$$I_R = R_\lambda \, S_\lambda \, D_\lambda \qquad [36]$$

were $R_\lambda$ is the reflectance coefficient $S_\lambda$ is the efficiency of the light source, and $D_\lambda$ the sensitivity of the detector for the reflected wavelength, $\lambda$. It has been shown that a variation of reflectance of $\simeq$ 2 % induces a detectable contrast (19).

For a **polychromatic** light source the situation is more complex and two parameters, hue and luminosity must be used and may be derived from experimental and calculated reflectance curves. The eye acuity is sensitive to both the hue and the luminosity simultaneously. The absolute value of the contrast detectable is a complex function (30). However, hue and luminosity can be considered separately to determine the minimum detectable limit resulting from variation of optical properties measured at different areas, characterized by reflectance variations versus wavelengths.

Let $\bar{x}_\lambda$, $\bar{y}_\lambda$ and $\bar{z}_\lambda$ be three sensitivity response factors for the detector (eye or photographic plate) corresponding to red, green, and blue regions respectively. For each of the three wavelength regions the measured intensity centered on the red, x, green, y, and blue, z, will be respectively :

$$x,y,z = \int_{\lambda_0}^{\lambda_1} (\bar{x}, \bar{y}, \bar{z}) \, S_\lambda \, R_\lambda \, d\lambda \qquad [37]$$

The values x, y and z define chromatic coordinates used to characterize the color of a specimen illuminated by a white light source according to the rule proposed by the Commission Internationale de l'Eclairage (CIE).

In practice, the chromatic coordinates are calculated using a discrete summation for the range of analyzed wavelengths :

$$x = \frac{\sum_\lambda \bar{x}_\lambda R_\lambda}{\sum_\lambda \bar{x}_\lambda R_\lambda + \sum_\lambda \bar{y}_\lambda R_\lambda + \sum_\lambda \bar{z}_\lambda R_\lambda}$$

$$y = \frac{\sum_\lambda \bar{y}_\lambda R_\lambda}{\sum_\lambda \bar{x}_\lambda R_\lambda + \sum_\lambda \bar{y}_\lambda R_\lambda + \sum_\lambda \bar{z}_\lambda R_\lambda} \qquad [38]$$

$$z = \frac{\sum_\lambda \bar{z}_\lambda R_\lambda}{\sum_\lambda \bar{x}_\lambda R_\lambda + \sum_\lambda \bar{y}_\lambda R_\lambda + \sum_\lambda \bar{z}_\lambda R_\lambda}$$

As discussed in (49), the color of the examined specimen is derived from the chromatic coordinates in

the chromatic chart (see Fig. 15). The light source is characterized by the coordinates ($x_o$, $y_o$).

The line passing from ($x_o$, $y_o$) through (x,y) intercepts the spectrum locus at a wavelength defining the hue of the specimen (see Figure 15). The hue is an average wavelength representing the observed color taking into account the energy sensitivity of the detector, the reflectance of the specimen and the energy distribution of the incident light.

The luminosity, i.e.,the intensity or brightness of the hue, is given by:

$$L(\%) = \frac{\sum_\lambda \bar{y}_\lambda R_\lambda}{\sum_\lambda \bar{y}_\lambda} \cdot 100 \qquad [39]$$

Thus, hue and luminosity are two single discrete parameters characterizing the shape and magnitude, respectively, of the reflectance curve (15).

**Contrast induced by luminosity changes**

The chromic oxide polishing procedure for $CuFeS_2$ following diamond polishing led to an increase in the reflectivity. Color calculations based on experimental data are shown in Table 4. Diamond and chromic oxide polished samples differ mainly in their luminosity while the hue remains about constant. This is consistent with data in Figure 4 where the curve shape is constant, but the reflectance is lower for diamond polishing.

Chromic oxide polishing was reported above to remove the silicone and sulfate compounds and reduced the iron oxide thickness. In fact, reflectance was measured as a function of time of polish with chromic oxide after first diamond polishing. The reflectance increased after each polishing sequence of 2 minutes and reached a constant reflectance after ≃ 10 to 15 minutes of chromic oxide polishing. It is therefore tempting to relate changes in reflectivity versus time of polishing to sequential uniform removal of the superimposed surface layers. It is difficult to justify such a model since the chromic oxide abrasives had an average diameter of 250 nm, while the total thickness of the surface layer(s) is $\lesssim$ 10 nm. It is questionable, therefore, whether 5 to 10 nm layers are sequentially and uniformly removed. An alternative and more viable explanation is that the chromic oxide polishing caused a variation with polishing time of the area fraction from which the silicone, sulfate and oxide layers were removed. This latter explanation is supported by the optical photomicrograph in Figure 12a which was recorded after 2 minutes of polishing with chromic oxide. Note that the surface is not uniform and exhibits local areas of different reflectivity. The number and dimensions of these areas increased with increasing polishing time up to 15 to 20 minutes. The contrast in the optical microscope thus results from changes in luminosity resulting from changes in surface layer thickness and composition. Topography effects induced by mechanical removal of surface compounds may also influence this contrast, but this does not seem likely. One effect of topography is to vary the level of the reflection surface, which because of the angle of the cone of the incident beam (≃/10° with the x 16 objective), will result in variations of illuminated area. If one considers that the maximum deviation from normal incidence when the objective used is only ± 5°, it can be shown that the defocusing effect could only change the contrast by 4.4 % even with a change of surface level equal to the maximum chromium oxide particle size (0.25 μm). As further evidence to support this calculation, if topographic defocusing was causing the contrast in Fig. 12a, then refocusing from the top to the bottom (and vice versa) of the topography would completely reverse the contrast in the image; this was not observed. Thus, the contrast in Figure 12a results largely from changes in reflectance, and the data in Table 4 show that this change is largely one of luminosity rather than hue. The data in Table 4 also show this change in luminosity results from changes in surface layer composition and thickness.

While the optical image shown in Fig. 12a demonstrates that chemical composition changes in a ≤ 10 nm surface layer affect the image, the same is true for secondary electron images of the surface (Fig. 12b).

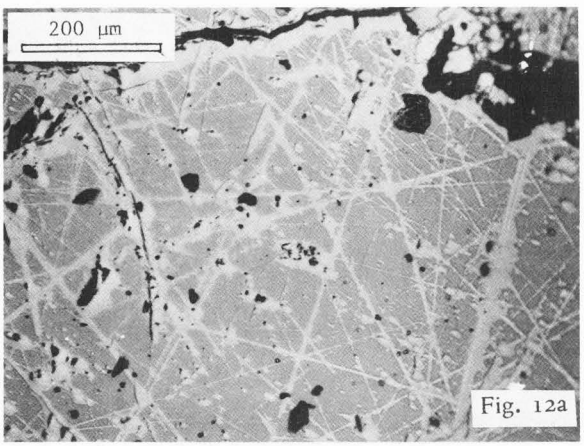


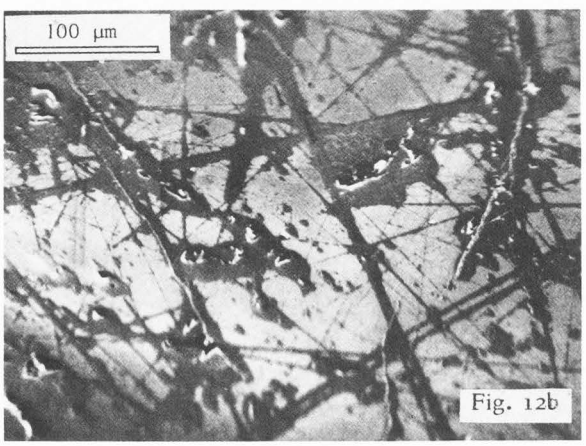


Fig. 12: Optical and scanning electron microscopy of a diamond polished chalcopyrite with iron oxide and copper rich sulfide layers partly removed by chromic oxide polishing for two minutes
a) optical microscopy (natural white incident light) and
b) secondary electron image (3 keV primary beam energy).

However the contrast is opposite between the optical and electron images shown in Fig. 12a and Fig. 12b respectively. In the optical microscope, the area where the iron oxide layer has been removed corresponds to higher reflectivity. The opposite contrast is observed by the SEM, i.e., the region with thicker iron oxide is brighter. Contrast in the secondary electron image is complex and the opposite contrast may arise from several factors (27).

Table 4 - Hue and Luminosity from Experimental and Calculated Reflectance Data for Polished Chalcopyrite

| Experimental Reflectance | | Hue (nm) | Luminosity (%) |
|---|---|---|---|
| Polishing Procedure | | | |
| Chromic Oxide | | 572 | 44 |
| Diamond | | 574 | 38 |
| **Calculated Reflectance** | | **Hue (nm)** | **Luminosity (%)** |
| $Fe_3O_4$ (nm) | $Cu_5FeS_4$ (nm) | | |
| 1 | 1 | 573.5 | 43 |
| 2 | 2 | 574.2 | 41 |
| 5 | 5 | 576.2 | 35 |
| 2 | 1 | 574.0 | 42 |
| 5 | 1 | 575.3 | 39 |
| 10 | 1 | 577.3 | 34 |
| 1 | 2 | 573.8 | 42 |
| 1 | 5 | 574.5 | 40 |
| 1 | 10 | 575.7 | 36 |

**Example of contrast by changes in both hue and luminosity**

For surface layer thickness $\geq$ 10 nm both the hue and luminosity will vary rapidly with the nature of the surface compounds and their spatial distribution. In some instances, polished chalcopyrite which had been stored in air for several months exhibited differently colored areas.

As previously discussed for natural tarnishing of chalcopyrite in air (5) the development of colored areas presumably results from an electrochemical oxidation mechanism assisted by residual water from polishing or adsorbed water from humidity in the air. By continued oxidation a thicker iron oxide layer and a deeper lying copper rich sulfide would be expected. If color changes are observed, the shape of the reflectance curve and thus the hue must change. This induces contrast in the optical image, which may be explained as follows. The reflectance curves from points 1 and 2 in Fig. 13 are shown in Fig. 14 and reduced to hue and luminosity in Fig. 15 and Table 5. Obviously the shape of the reflectance curves for the two points is different, consistent with a change in color and therefore changes in both hue and luminosity. It may occur to the reader that the contrast which is observed and obviously related to crystallography dependence may result from differences in crystallographic orientation in the chalcopyrite substrate. However, crystal orientation is only observed for reflected light which was polarized prior to striking the sample **and** crossed-polarized after reflection. For Fig. 13 the incident light was polarized, but the reflected light was not crossed-polarized. Thus, the contrast must result from effects other than crystallographic orientation changes of the $CuFeS_2$. The color difference on the sample in Fig. 13 results from differences in the thickness of the iron oxide and/or the copper rich sulfide layers. This is demonstrated by the reflectance curves shown in Fig. 16a and Fig. 16b, which were calculated assuming either a 10 nm or 25 nm single layer of $Fe_3O_4$ was present on the surface. The same conclusion may be drawn if FeO.OH was the oxide on the surface, or if a bornite layer was present with the oxide. Note that two calculated reflectance curves are shown for each layer thickness. Fig. 16a represents the reflectance for chalcopyrite covered with $Fe_3O_4$ layers calculated by subsituting in equation [18] the reflectance for the substrate by each of the extreme $R_o$ and $R_e$ reflectance for chalcopyrite successively. This situation is equivalent to that of a substrate consisting of two chalcopyrite crystals with perpendicular optical axes. Neglecting the weak anisotropy of the chalcopyrite, Fig. 16b shows the calculated reflectance curves considering the maximum $R_g$ and the minimum $R_p$ reflectance of the FeO.OH surface layer successively.

Since the differences in the calculated curves from crystals with perpendicular optical axes is small compared to the differences resulting from changes in the surface layer thickness, the color change in Fig. 13 results from changes in the oxide thickness, not from anisotropy of chalcopyrite. This conclusion is further supported by the fact that optical anisotropy of chalcopyrite results in less than 2 % variation of reflectance, and Françon (19) has shown that reflectance changes of less than 2 % are not detectable. As a result, it is concluded that the oxidation rate of chalcopyrite is a function of crystallographic orientation, and differences in orientation may be revealed by differences in oxide thicknesses.

Table 5 - Color calculation at the locations 1 and 1 and 2 shown in the optical photomicrograph in Fig. 13 .

| Analyzed area | Hue nm | Luminosity % |
|---|---|---|
| Area 1 | 576.0 | 33.2 |
| | 576.2 | 28.9 |
| Area 2 | 582.5 | 15.9 |
| | 582.3 | 14.7 |

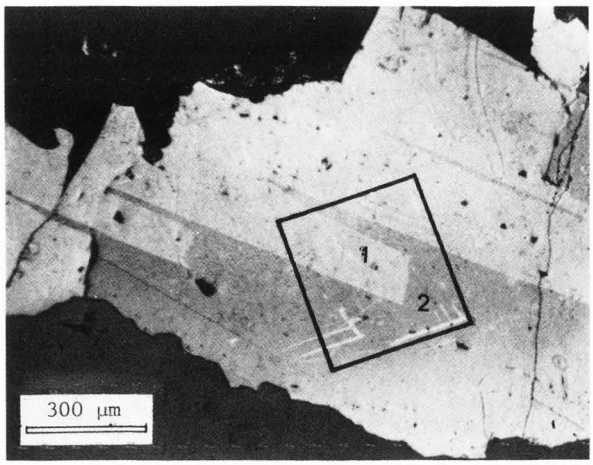


Fig. 13: Optical examination of a chalcopyrite exposed to laboratory air for several months (linearly polarized incident light, not-crossed polarized reflected light). The colored areas, 1 and 2, correspond to differences in crystallographic orientations of the chalcopyrite substrate as shown by optical examination with crossed-polarized reflected light after the specimen was repolished.

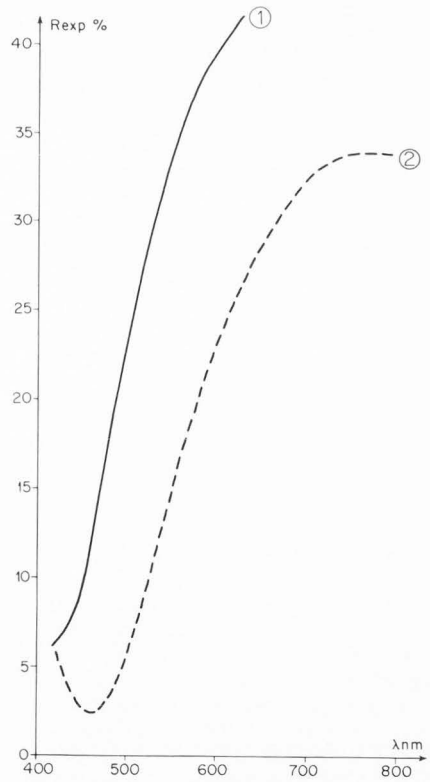


Fig. 14: Experimental reflectance curves at locations 1 and 2 shown in Fig. 17.

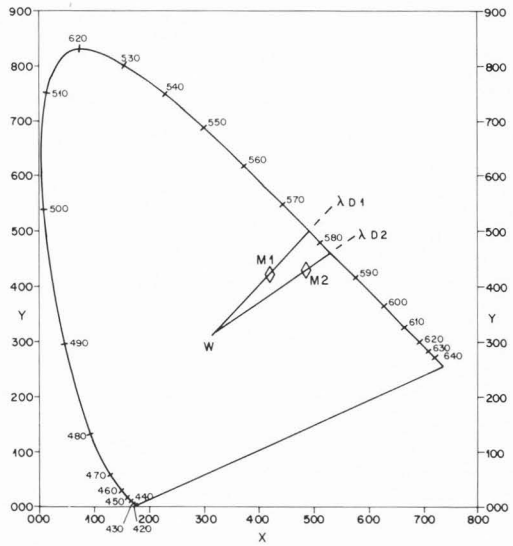


Fig. 15: Chromatic chart indicating hue changes derived from the experimental reflectance curves measured at the different colored areas shown in Fig. 13.

**Detection limit in thickness variations of surface layers**

Since optical contrast can result from changes in hue and/or luminosity, it is interesting to consider the minimum thickness difference which can be recongized in optical images and microreflectometry measurements. Ruzakowski et al. (43) reported that layers as thin as 0.5 nm (for $Ag_2S$ on chalcopyrite) were detectable by reflectance measurements. To determine the minimum $Fe_3O_4$ thickness difference leading to detectable contrast, the percent change in hue or luminosity was calculated and is shown in Fig. 17. For the calculation, $CuFeS_2$ was assumed to have either no $Fe_3O_4$ or a 40 nm thick $Fe_3O_4$ layer on the surface ($z_o$ in Fig. 17). An adjacent area was then assumed to have a thickness different from $z_o$ by $\Delta_z$. As reported above, 2 % changes in luminosity are detectable, therefore optical contrast on chalcopyrite surfaces will be observed for 1 nm of $Fe_3O_4$ adjacent to clean $CuFeS_2$. For $CuFeS_2$ covered by 40 nm of $Fe_3O_4$, a thickness of 42 nm ($\Delta_z$ = 2 nm) will result in contrast by changes in luminosity. For a given $\Delta_z$ the relative variations in hue and luminosity are a function of the $Fe_3O_4$ thickness. For $z_o$ = 0 nm, the luminosity is much more sensitive to $\Delta_z$ than is hue, but at $z_o$ = 40 nm, hue is more sensitive than is luminosity at low $\Delta_z$.

The variation in crystal orientation shown by contrast due to various thicknesses of oxide on chalcopyrite developed after a few months in air (see Fig. 13) can also be seen in a much shorter air exposure.

An example is shown in Fig. 18 where chalcopyrite was sputtered with 3keV $Ar^+$ in the Auger spectrometer. After sputtering, the sample was stored in laboratory air for two days, then observed by optical microscopy. As shown in Fig. 18 the variation in crystal orientation is obvious for the sputtered area, but not apparent in the area which was not sputtered. As for the sample in Fig. 15 the incident light was polarized but the

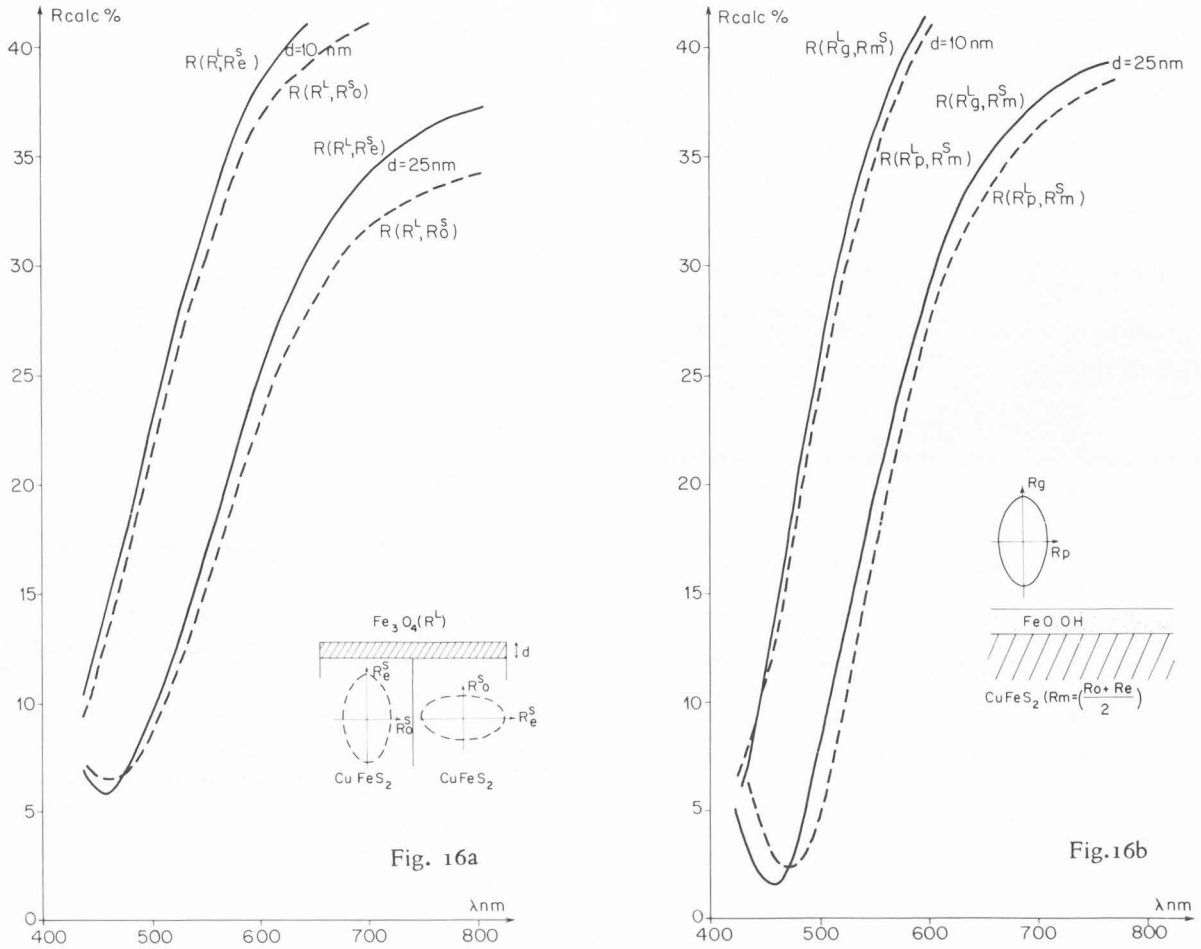


Fig. 16a

Fig.16b

Fig. 16: Calculated reflectance curves for chalcopyrite of 10 and 25 nm in thickness successively covered with a homogeneous iron oxide layer.

a) effects of anisotropy of the chalcopyrite ($R_o$, $R_e$) covered with a $Fe_3O_4$ isotropic layer.

b) effects of anisotropy of the FeO.OH surface layer ($R_p$, $R_g$) neglecting the anisotropy of the chalcopyrite substrate characterized by its average reflectance $R_m = (R_o + R_e) / 2$.

reflected light was not crossed-polarized, therefore the crystallographic structure must result from variations in the oxide layer thickness or topography. Ion sputtering may induce surface topography which varies with crystal orientation (24). Topography should cause a decrease in luminosity, but have little change in hue. However the data in Fig. 17 show a similar effect on luminosity and hue for small thickness change in thin surface layers. For the areas shown in Fig. 18 the hue is the same for measurements on or off of the ion exposed area .The crystal orientation contrast results from changes in luminosity. Therefore, the contrast must result from either topography or from thickness changes in thin surface layers. We will use electron spectroscopy and microscopy to show that the contrast results from variations in thickness of the oxide surface layer.

The crystallographic contrast shown in Fig. 13 and Fig. 18 are similar, yet that in Fig. 15 was observed after several months in air, while that in Fig. 18 was observed only after two days. The contrast in both cases result, however from variations in the oxide, therefore the oxidation rate after ion sputtering must be significantly greater than for polished surfaces. This is reasonable since many studies have shown that ion sputtering accelerates the rate of oxidation and both accelerated and non accelerated oxidation rates vary with crystal orientation (21) (23).

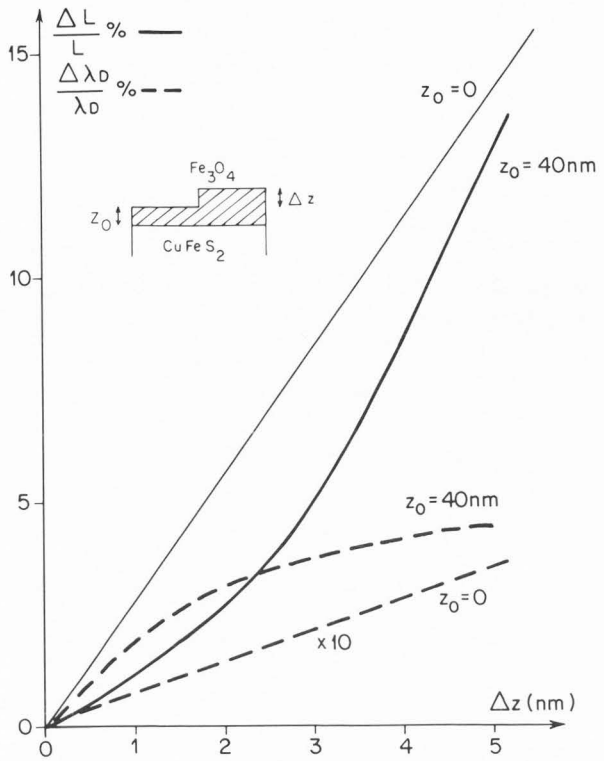


Fig. 17: Percent variations in hue and luminosity as a function of the thickness variations $\Delta_z$ of a $Fe_3O_4$ layer with thickness $z_o$ on top of chalcopyrite.

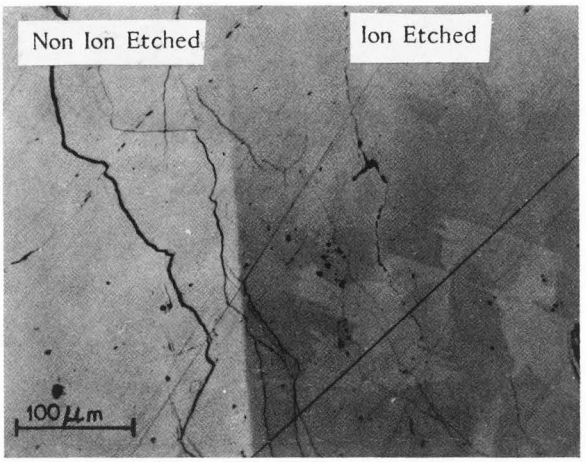


Fig. 18: Optical microscopy (linearly polarized incident light, not-crossed-polarized reflected light) of a polished chalcopyrite surface partly exposed to iron bombardment and stored in laboratory air for two days.

## Comparisons between optical and electron images

In optical microscopy, the illumination is usually produced by white light source. Thus, the reflected light is polychromatic and the contrast results from both hue and luminosity as discussed above. In scanning electron microscopy, the illumination is produced by a monoenergetic incident electron beam of intensity, $I_p$. The brightness of the image, B, has been shown to vary linearly with the total emission current, $I_s = I_p - I_a$ where $I_a$ is the absorbed current (29). Similarly, it has also been shown that a linear relationship exists between B and the integrated electron energy distribution, S, given by:

$$S = \int_{Ep}^{o} n(E)\, dE \qquad [40]$$

where n(E) is the number of emitted electrons with energy (E). Only the fraction, $\delta_E.S_E$, of emitted electrons produce signals at the output of the detector. The parameter $\delta_E$ is a characteristic of the detector including its spectral response function, its acceptance angle etc... (28) (35). Thus, for a monoenergetic incident electron beam, the contrast of the electron image, $\Delta B/B$, is proportional to the differentiated integrated energy distribution $\Delta S/S$. The situation is similar to that occurring in optical microscopy when the specimen is illuminated a white source ($S_\lambda$) the reflected intensity being measured by a detector characterized by a single sensitivity factor ($D_\lambda$).

Thus, changes in the intensity of the total number of emitted electrons without changes in the shape of the electron energy distribution n(E) would lead to a contrast equivalent to the optical contrast due to luminosity changes. Changes in both intensity and shape of the n(E) distribution would lead to a contrast equivalent to the contrast resulting from hue and luminosity changes in optical microscopy.

Photomicrographs, taken in reflected light and in a scanning electron microscope were obtained from a different area of the polished section shown in Fig. 13 are given in Fig. 19a and Fig. 19b. The optical image was recorded with plane-polarized incident light but not-crossed polarized reflected light. The contrasts observed in Fig. 19a coïncide with crystallographic orientations changes of the chalcopyrite as shown by optical examination with crossed polars after the surface was ion sputter-cleaned (see Fig. 20). The contrast shown in Fig. 19b may result from an electron channeling effect due to different crystallographic orientations of the polycrystalline chalcopyrite. Channeling effects have been discussed for backscattered electron images (33), for secondary electron microscopy (28) and Auger spectroscopy (2). However, as discussed earlier, the contrast seen in optical photomicrograph (Fig. 19a) as changes in hue results largely from variations in thickness of the oxide layer at the surface of the chalcopyrite crystals. Contrast over the same area is obvious in the secondary electron image (Fig. 19b) but the light and dark areas are reversed. Points 1 and 2 in Fig; 19b were analyzed using stationary beam Auger depth profiles and the oxide was thicker at point 1. The secondary electron image of the sputter-cleaned surface exhibited a very weak contrast. Therefore, we conclude that oxide thickness can result in contrast in both optical and electron images.

To further explore the idea that thickness variations of oxide layers produce contrast in electron images, the sputter-cleaned sample in Fig. 19b was removed from the vacuum and exposed to laboratory air for a few hours. Optical photomicrographs were taken, and the sample was imaged in a scanning electron microscope. According to Stern (46) the channeling effect must be present in all regions of the energy distribution of the emitted electrons. Thus, in order to determine whether the contrast in electron images is preferentially due to a channeling effect or to thickness variations of surface layers, secondary and backscattered electron images were compared. A solid state backscattered electron detector was used. As shown in Fig. 17 the oxide thickness variation ($\Delta_z$ in Fig. 17) was not sufficient after this period of exposure to air to reveal differences in crystal orientations for the chalcopyrite substrate with plane-polarized light (Fig. 20a). However, the crystal orientations for the area are the same as in Fig. 19 as seen under conditions of plane-polarized light and crossed polars in Fig. 20b (Note that the contrast in Fig. 20b would reverse by rotating the specimen 90° relative to the analyzer). The crystallographic changes in orientation also are not visible in scanning electron images taken with a primary beam energy of 4 keV (Fig. 20f) but could be observed for beam energies of 0.6, 0.8 and 1 keV as shown in Fig. 20c, d and e respectively.

The thickness variations of the oxide layer, which was assumed to be too thin to induce a change in hue or luminosity (Fig. 20a) may be large enough to induce a contrast in the backscattered electron image (Fig. 20b). However, the contrast may be made visible by a thickening of the oxide layer, due to an increase in the rate of oxidation when exposed to air after electron beam irradiation of the sputter-cleaned surface, as reported by Bischke et al. for aluminum oxidation (1). Moreover, Fontaine et al. showed that an aluminum crystal (1.1.1.) exposed to oxygen exhibited a higher oxidation rate under electron irradiation than similarly exposed aluminum (1.0.0) crystal (18).

To understand the reasons for observing contrast in secondary and backscattered electron images due to variations in oxide thickness, the backscattered coefficient for chalcopyrite will be considered as discussed for the optical reflectance coefficient for chalcopyrite. A review of electron backscattering for thin film and multilayers has been given by Niedrig (34). Cosslet and Thomas (17) evaluated the current transmitted across a boundary at a depth, x, using a multiple reflection model analogous to the optical treatment. For a thin surface layer on a substrate, a simplified expression for the effective backscatter coefficient, $\eta_{eff}$, was given by Rydnik and Borovskii (44) as reported in (42).

$$\eta_{eff} = \eta_s \frac{n_{\rho z}}{n_o} + \eta_L \left(1 - \frac{n_{\rho z}}{n_o}\right) \qquad [41]$$

where $\eta_s$ and $\eta_f$ are the backscatter coefficients for substrate and surface film respectively, and $n_o$ and $n_{\rho z}$ are the number of electrons at the surface and a mass depth of $\rho z$ respectively; $\rho$ is the density and z is the linear depth. It is generally assumed that the number of

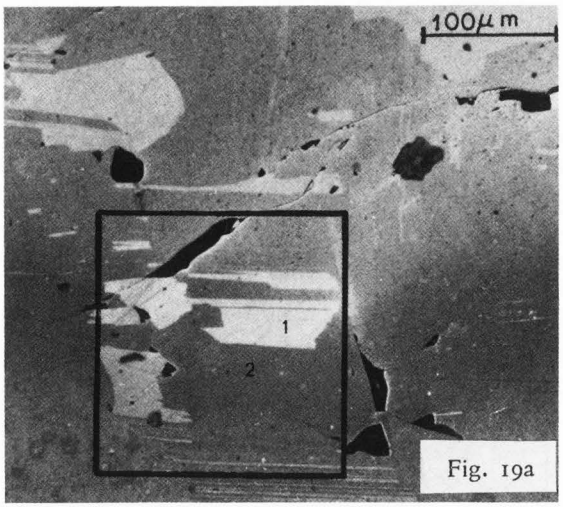


Fig. 19a

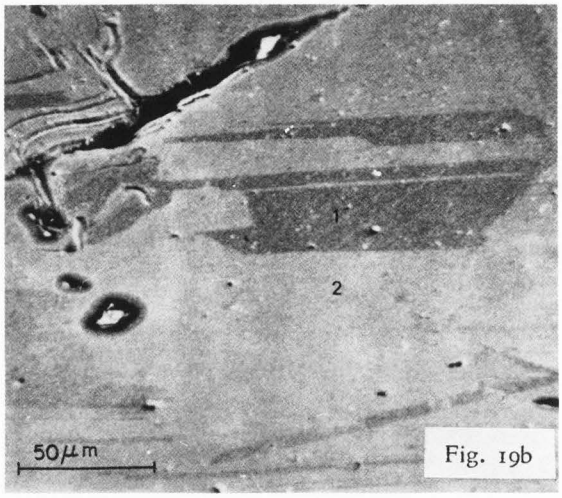


Fig. 19b

Fig. 19: Comparisons between optical and secondary electron images of a naturally oxidized chalcopyrite surface
a) Optical photomicrograph: (linearly-polarized incident light, not-crossed-polarized reflected light)
b) secondary electron image: 5 keV primary beam energy.

Fig. 20: Specimen as shown in Fig. 22 after $Ar^+$ ion etching and air exposure for two days.
a) Optical microscopy: linearly-polarized incident light, not-crossed polarized reflected light (The image is rotated 90° relative to the image in Fig. 22)
b) Optical microscopy: linearly-polarized incident and crossed-polarized reflected light showing crystallographic orientation differences of the chalcopyrite specimen
c) d), e), f) backscattered electron images 0.6 keV (C), 0.8 keV (d), 1 keV (e) and 4 keV (f) primary beam energy.

→

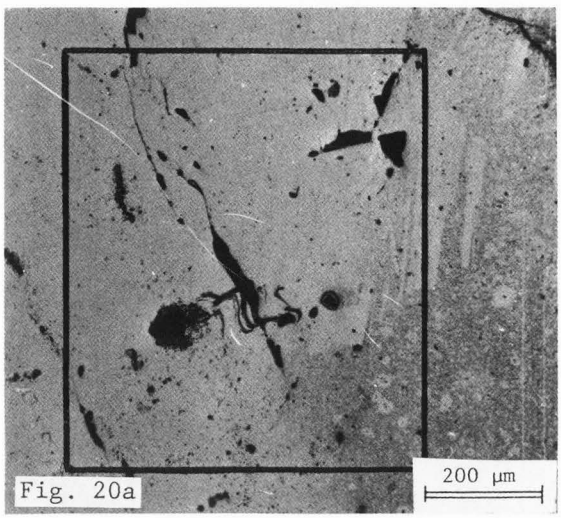

Fig. 20a

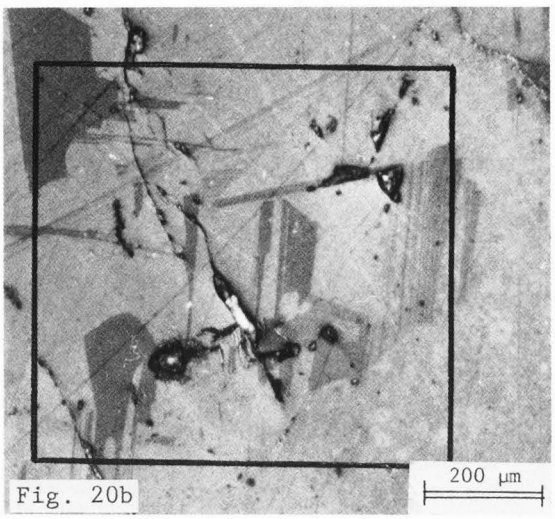

Fig. 20b

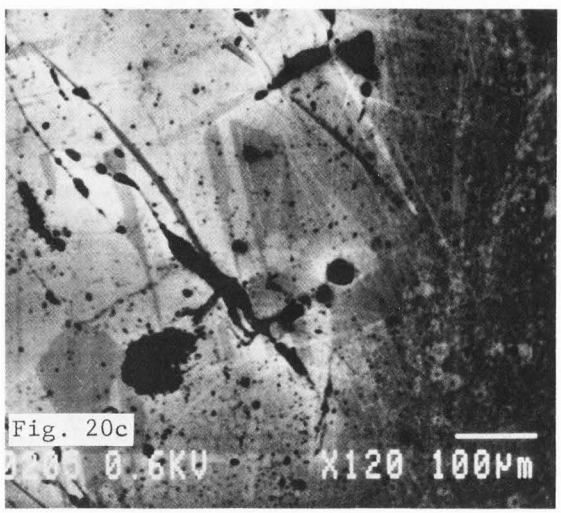

Fig. 20c

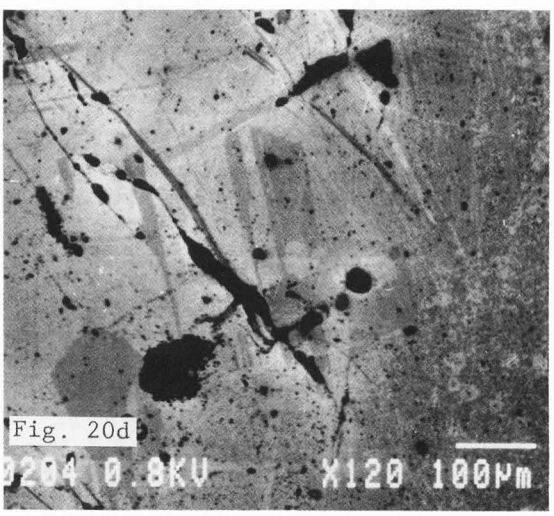

Fig. 20d

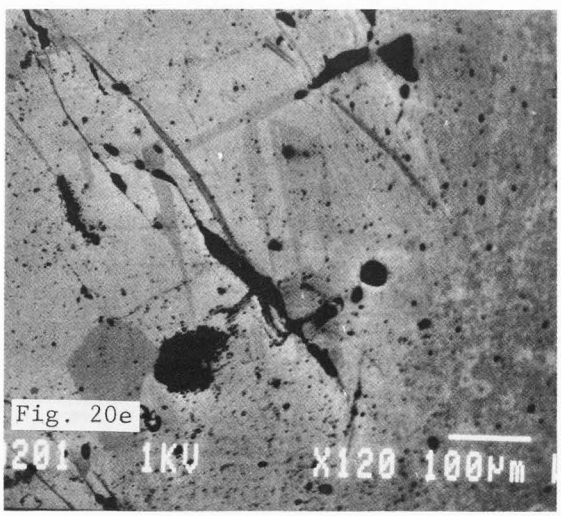

Fig. 20e

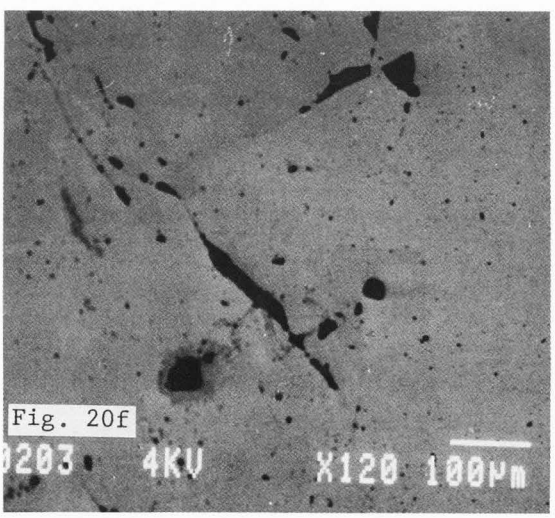

Fig. 20f

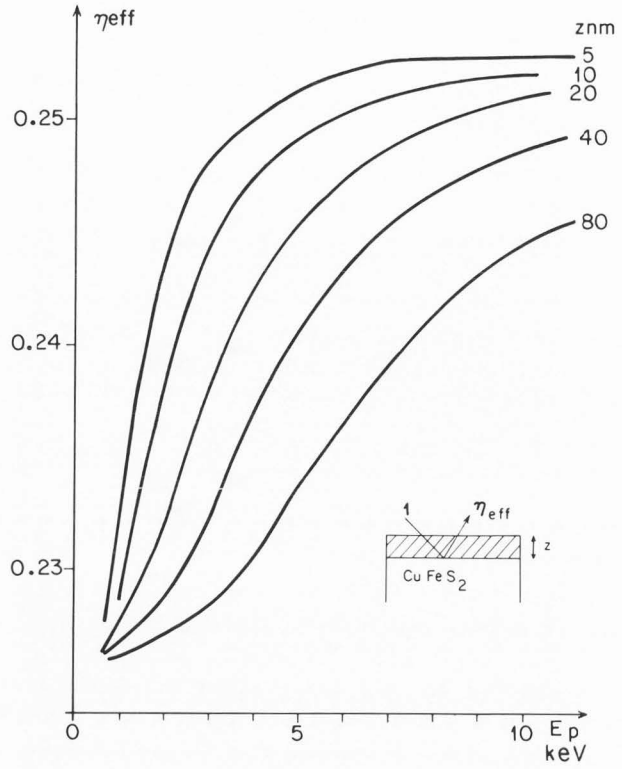


Fig. 21: Calculated effective electron backscatter coefficient vs primary beam energy for a chalcopyrite covered with a $Fe_3O_4$ layer of different thicknesses.

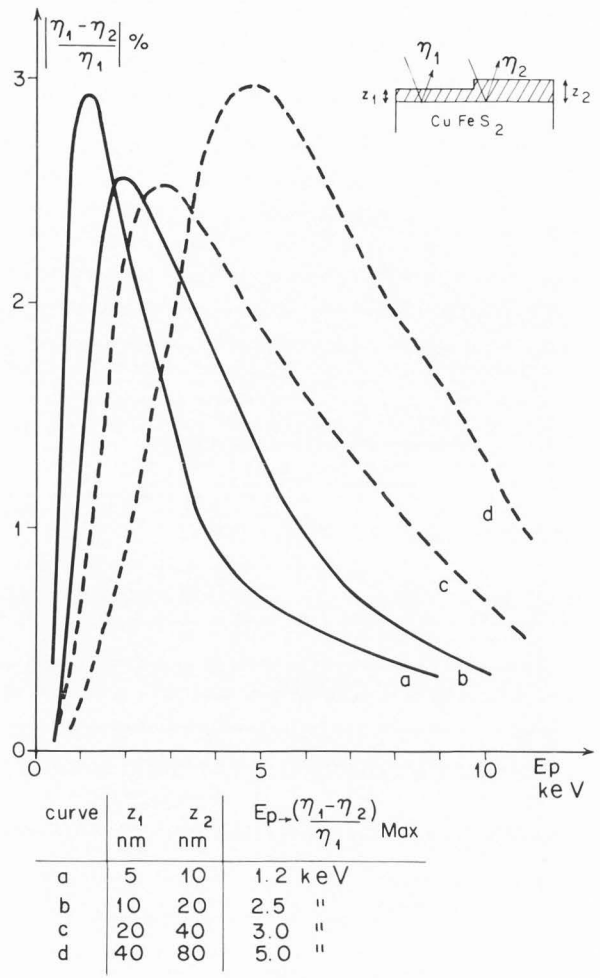


| curve | $z_1$ nm | $z_2$ nm | $E_p \rightarrow \frac{(\eta_1-\eta_2)}{\eta_1}$ Max |
|---|---|---|---|
| a | 5 | 10 | 1.2 keV |
| b | 10 | 20 | 2.5 " |
| c | 20 | 40 | 3.0 " |
| d | 40 | 80 | 5.0 " |

Fig. 22: Variations with the primary beam energy of the percent difference $(\eta_1 - \eta_2) / \eta_1$ for the effective backscatter coefficients of a chalcopyrite covered with a $Fe_3O_4$ layer with thickness varying from $z_1$ to $z_2$.

electrons at a depth, $\rho z$, below the surface is described by an exponential decay

$$n_{\rho z} = n_o \exp(-\sigma \rho z) \qquad [42]$$

where $\sigma$ is the Lenard's coefficient. For a primary beam energy ranging from a few keV to a few tens of keV, as used in X-ray spectrometry with the electron probe micro-analyzer, the usual expression for $\sigma$ is (22):

$$\sigma = \frac{4.5\ 10^5}{E_p^{1.65}} \qquad [43]$$

The backscatter coefficients $\eta_s$ and $\eta_f$ may be expressed according to the usual polynomial relation from Heinrich (22):

$$\eta = 0.0254 + 0.016\ Z - 0.000186\ Z^2 + 8.3\ 10^{-7}\ Z^3 \qquad [44]$$

where Z is the atomic number of the element for a complex compound:

$$\eta = \sum_i C_i\ \eta_i \qquad [45]$$

and $C_i$ is the weight fraction of the elements in the substrate or the film.

Using equation [41], $\eta_{eff}$ for a chalcopyrite substrate, covered with an $Fe_3O_4$ surface layer, can be calculated using $\rho = 5.2$ g/cm$^3$ for magnetite.

Results in Fig. 21 show the variation of $\eta_{eff}$ as a function of the primary beam energy $E_p$ and different thicknesses of the oxide layer. These calculation give the total number of backscattered electrons independent of their energy distribution. However, the contrast in the backscattered electron image will be proportional to the relative difference in emission, $d\eta/\eta$, of the backscattered electrons at two different locations. Assuming a relative thickness variation of 50 %, variations in $d\eta/\eta$ were calculated and shown in Fig. 22. These results show that there is a particular value of the incident energy leading to a maximum of contrast and that this critical energy is a function of the thicknesses of the layers. These variations of $d\eta/\eta$ are consistent with results of Boiziau et al. (3) who showed that a critical thickness of aluminum oxide at the surface of an aluminum substrate would result in a maximum of electron emission for a particular primary

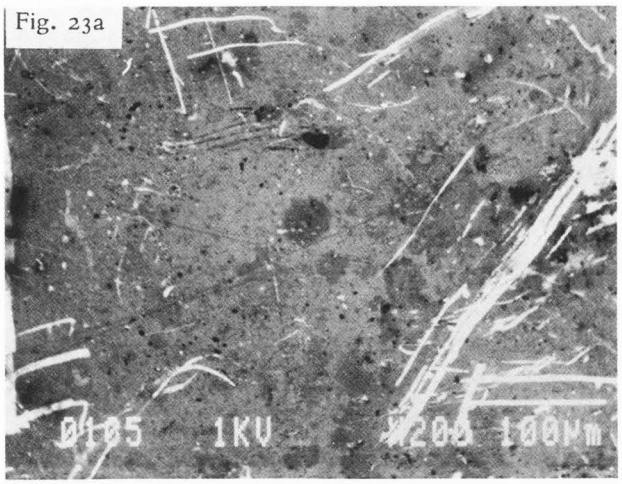


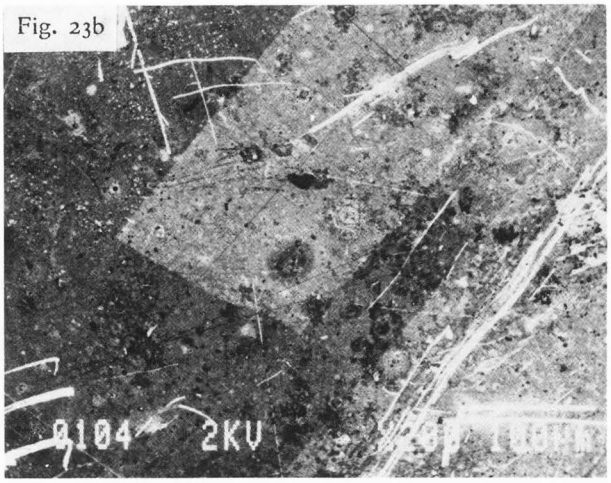


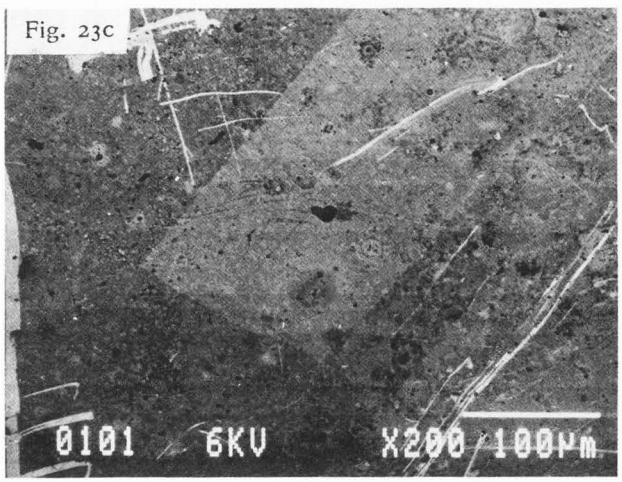


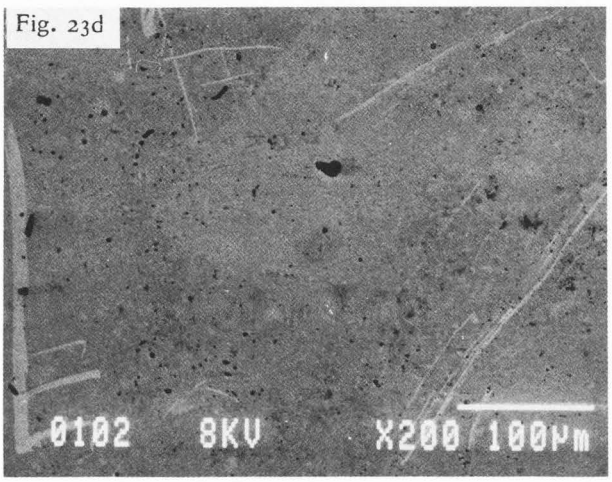


Fig. 23: Backscattered electron images of the area shown on the optical photomicrograph in Fig. 17: 1 keV (a), 2 keV (b), 6 keV (c) and 8 keV (d) incident beam energy.

energy. Based on these results, if the surface layer varies in thicknesses such that contrast is observed in the SEM, this contrast should be a function of the primary beam energy. This variation in contrast with beam energy was shown above by Fig. 20 and a second example is shown in Fig. 23 for the same areas as previously illustrated in Fig. 13. The data shown in Fig. 23 demonstrates good contrast at a primary beam energy of 2 keV, with little contrast at 1 and 8 keV. The calculated and experimental reflectance data for the areas in Fig. 13 were shown earlier (Fig. 16a and Fig. 16b) and the conclusion drawn that the $Fe_3O_4$ layer was 10 and 25 nm thick in the light and dark areas, respectively. The data for case b in Fig. 22 shows that a maximum contrast should occur for layers 10 and 20 nm thick at a beam energy of $\sim$ 2.5 keV, which is remarkably consistent with the images in Fig. 23. Chalcopyrite specimens covered with oxide films, when observed with polarized incident light exhibited crystallographic contrasts identical to those which should be obtained when observing a non oxidized chalcopyrite surface under crossed polar conditions. For specimens covered with oxide films, the contrast resulting from local changes in hue and/or luminosity was associated with differences in thickness of the layer depending on crystallographic orientation of the underlying chalcopyrite crystals. The same features were shown in secondary electron images, but the contrast between optical and secondary electron images was reversed. In the backscattered electron images, contrast was only present for the same critical values of the primary beam energy and was identical to that observed in optical images. Thus, the contrast observed in both the secondary and the backscattered electrons images results from variations in thicknesses of the oxide surface film rather than from a channeling effect. Therefore, it is obvious that thin surface layers may affect not only the optical image, but also affect the secondary and backscattered electron images.

## Summary

The effect of surface composition upon reflectance from mineral surfaces has been discussed. A general model incorporating the effects of multiple thin surface layers of absorbing material covering a substrate of absorbing material was developed. Expressions were given for multiple uniform layers on a substrate (homogeneous model) and for two materials uniformly mixed in a single surface layer (heterogeneous model). For the heterogeneous model, expressions were developed for the reflectance coefficient both for light only traveling through a single phase (independent sources) and traveling first through one and then the other phase (dependent source).

This model was used to calculate reflectance curves for polished chalcopyrite ($CuFeS_2$) with thin surface compounds. The types of surface compounds and their approximate thicknesses were defined by measuring polished surfaces with X-ray photoelectron and Auger electron spectroscopies. Incorporating these data into the calculated reflectance curves, the comparison between experiment and theory was very good. The hue and luminosity were determined for calculated and experimental reflectance curves and these parameters proved to be useful single value reflectance data which could also be used to characterize surface chemistry. Contrast in optical photomicrographs was discussed and it was shown that surface chemistry dominates this contrast for polished $CuFeS_2$. Contrast due to both changes in hue (color) and luminosity (brightness) were illustrated. The relationship between the contrast observed by optical microscopy or observed on the same sample by electron imaging was illustrated and discussed using a model to calculate electron backscatter coefficient, it was shown that contrast due to film thickness variation was important and was a function of primary beam energy. Using experimental data, the dependence of electron image contrast upon primary beam energy was shown to be consistent with optical determination of surface layer thickness variations. As a result, it was concluded that optical reflectance can be used for surface analysis, and that optical and electron images can be influenced by thin surface layers.



## Acknowledgements

This work was supported by NSF Grant CPE 82178839 (PHH and PR) and by CEE Grant MSM - 043 F (GR, RC, CG).


## References


(1) Bischke SD, Oen AC, Falconer JL.(1984) - Electron beam effects on the rate of aluminium oxidation by carbon dioxide; Appl. Surf. Sci. 20 (1-2), 97-108.

(2) Bishop HE, Chornik B., Le Gressus C., Le Moel A. (1984) -Crystalline effects in Auger electron spectroscopy; Surf. and Interface Analysis, 6, n° 3, 116-128.

(3) Boiziau C., Duraud JP, Le Gressus C., Massignon D. (1983) - Ultra high vacuum analytical Scanning Electron Microscopy: An interpretable secondary electron image for surface science. Scanning Electron Microsc., 1983; IV: 1525-1534.

(4) Buckley RG, Beaglehole D. (1977) - Absorptance of thin films. Applied optics, 16, n° 9, 2495-2499.

(5) Caye R. (1973) - "Contribution au développement de la microréflectométrie sous incidence oblique pour l'étude des minéraux," Thesis, University of Paris VI.

(6) Caye R., Cervelle DB.(1968) - "Détermination de l'indice de réfraction et du coefficient d'absorption des minéraux non transparents." Bull. Soc. Fr. Mineral. Cristallogr. (1968), 91, 284-288.

(7) Caye R., Pasdeloup J. (1977) - Reference reflectance data for bornite, International Mineralogical Association, Commission on Ore Microscopy, Quantitative data file. The Applied Mineralogy group of the Mineralogical Society, 41 Queen's Gate, London, England, card n° 1.1020-2.

(8) Caye R., Pasdeloup J. (1977) - Reference reflectance data for chalcopyrite, International Mineralogical Association, Commission on Ore Microscopy, Quantitative data file. The Applied Mineralogy group of the Mineralogical Society, 41 Queen's Gate, London, England, card n° 1.1500.2.

(9) Caye R., Pasdeloup J. (1977) - Reference reflectance data for magnetite, International Mineralogical Association, Commission on Ore Microscopy, Quantitative data file. The Applied Mineralogy Group of the Mineralogical Society, 41 Queen's Gate, London, England, card n° 1.5220.1.

(10) Caye R., Pasdeloup J. (1977) - Reference reflectance data for wustite, International Mineralogical Association, Commission on Ore Microscopy, Quantitative data file. The Applied Mineralogy group of the Mineralogical Society, 41 Queen's Gate, London, England, card n° 1.

(11) Caye R., Pasdeloup J. (1977) - Reference reflectance data for goethite, International Mineralogical Association, Commission on Ore Microscopy, Quantitative data file. The Applied Mineralogy group of the Mineralogical Society, 41 Queen's Gate, London, England, card n° 1.3180.

(12) Caye R., Pasdeloup J. (1977) - Reference reflectance data for hematite, International Mineralogical Association, Commission on Ore Microscopy, Quantitative data file. The Applied Mineralogy Group of the Mineralogical Society, 41 Queen's Gate, London, England, card n° 1.3640.

(13) Cervelle DB, Caye R., Billard J. (1970) - Détermination des indices de cristaux uniaxes fortement absorbants. Application à la pyrrhotite hexagonale. Bull. Soc. fr. Mineral. Cristallogr., 93, 72-82.

(14) Cervelle DB, Levy C. (1971) - "Propriétés optiques de la covelline et de l'énargite dans le visible et dans l'unifro rouge proche", Bull. Soc. fr. Mineral. Cristallogr., 94, 146-155.

(15) Cervelle DB, Malezieux JM, Caye R. (1977) - Expression quantitative de la couleur liea à la reflectance diffuse de quelques roches et minéraux, Bull. Soc. fr. Mineral. Cristallogr., 100, 185-191.

(16) Chen TT, Dutrizac JE, Owens DR, Laflamme JHG. (1980) - Accelerated tarnishing of some chalcopyrite and tennantite specimens, Canadian Mineralogist, 18, 173-180.

(17) Cosslett VE, Thomas RN. (1965) - Multiple scattering of 5-30 keV electrons in evaporated metal films III: Backscattering and absorption. Brit. J. Appl. Phys., 16, 779-796.

(18) Fontaine JM, Lee-Deacon O., Duraud JP, Ichimura S., Le Gressus C. (1982) -Electron beam effects on oxygen exposed aluminium surface, Surface Science, 122, 40-54.

(19) Françon M. (1954) - Le microscope à contraste de phase et le microscope interférentiel, Les Editions du CNRS, p. 45.

(20) Galopin R., Henry NMF.(1972) - Microscopic study of opaque minerals, Published by W. Heffer and Sons Ltd, Cambridge; G.B., 83-103.

(21) Gonzalez L., Miranda R., Ferrer S. (1982) - The effect of Argon bombardment on the oxidation of Fe(110) by oxygen and water. Solid State Communications, 44, n° 10, 1461-1463.

(22) Heinrich KFJ. (1981) - Electron beam X-ray Microanalysis, Van Nostrand Reinhold Company, NY, 219-302.

(23) Holloway PH. (1981) - Chemisorption and oxide formation on metals: oxygen-nickel reaction; J. Vac. Sci. Technol., 653-659.

(24) Holloway PH, Bahattacharya R. (1981) -Limitations of ion etching for interface analysis, Surface and Interface Analysis, 3, 118.

(25) Holloway PH, Remond G., Swartz WE. (1982) - Electron spectroscopy and optical microreflectometry of polished sulfide minerals, in Proc. of Conference in: Interfacial Phenomena in Mineral Processing, Yarar B., Spottiswood DJ (eds.), Engineering Foundation, 345 E. 47th Street, New York, 93-117.

(26) Hummel RE. (1985) - Electronic Properties of Materials: An Introduction for Engineers. Springer-Verlag New-York Inc., 175 fifth Avenue New-York, NY 10010, 320 pp.

(27) Lee-Deacon O., Le Gressus C., Massignon D. (1982) -Analytical scanning electron microscopy for surface science, in: Electron Beam Interactions with Solids for Microscopy, Microanalysis and Microlithography, Kyser D.F., Niedrig H., Newbury DE and Shimizu R (eds), SEM Inc., AMF O'Hare, Il 60666. USA, 271-280.

(28) Le Gressus C., Duraud JP, Massignon D., Lee-Deacon O. (1983) - Electron channeling effect on secondary electron image contrast. Scanning Electron Microsc., 1983; II: 537-542.

(29) Le Gressus C., Okuzumi H., Massignon D. (1981) - Changes of secondary electron image brightness under electron irradiation as studied by electron spectroscopy. Scanning Electron Microsc. 1981; I: 251-261.

(30) Mac Adam DL.(1949) - Color discrimination and the influence of color contrast on visual acuity, Rev. Opt., 28, 161.

(31) Mouchart J. (1977) - Thin film optical coatings. 3: Two wavelength antireflection coatings. Applied Optics, 16, n° 11, 3001-3008.

(32) Mouchart J. (1977) - Thin film optical coatings. 4: Multilayer antireflection coatings. Applied Optics, 16, n° 12, 3237-3241.

(33) Newbury DE (1977) - Fundamentals of scanning electron microscopy for physicist: contrast mechanisms, Scanning Electron Microsc., 1976; I: 553-568.

(34) Niedrig H. (1982) - Analytical models in electron backscattering; Electron beam interactions with solids for microscopy, microanalysis and microlithography, in: Electron Beam Interactions with Solids for Microscopy, Microanalysis and Microlithography. Kyser DF, Niedrig H., Newbury DE, and Shimizu R. (eds), SEM Inc, AMF O'Hare, Il 60666, USA, 51-68.

(35) Reimer L. (1982) - Electron signal and detector strategy. in: Electron Beam Interactions with Solids for Microscopy, Microanalysis and Microlithography. Kyser DF, Niedrig H., Newbury DE and Shimizu R. (eds), SEM Inc, AMF O'Hare, IL 60666, USA, 299-310.

(36) Remond G., Giraud R., Holloway PH, Packwood RH. (1984) - The effect of volume and surface diffusion of impurities on the detection limit in microprobe analysis; Scanning Electron Microsc. 1984; I: 151-166.

(37) Remond G., Giraud R., Holloway PH, Packwood RH, Taylor JA.(1984) - X-ray and Auger electron spectroscopies applied to the study of tarnished ZnS surfaces, Proc. 2nd International Conference on Applied Mineralogy, The Metallurgical Society of AIME, 67-87.

(38) Remond G., Holloway PH, Hovland CT, Olson RR. (1982) - Bulk and surface silver diffusion related to tarnishing of sulfides; Scanning Electron Microsc. 1982; III: 995-1011.

(39) Remond G., Holloway PH, Le Gressus C. (1981) - Electron spectroscopy and microscopy for studying surface changes of mechanically prepared pyrite and quartz, Scanning Electron Microsc. 1981; III: 482-492.

(40) Remond G., Kosakewitch A., Holloway PH, Ruzakowski P., Packwood RH, Taylor JA. (1984) - "X-ray spectrometry, electron spectroscopies and optical microreflectometry applied to the study of ZnS tarnishing in polished ore sulfide specimens, Scanning Electron Microsc. 1985; IV: 1305-1326.

(41) Remond G., Picot P., Giraud R., Holloway PH, Ruzakowski P. (1983) -Contribution of electron spectroscopies and X-ray spectrometry applied to the geosciences. Scanning Electron Microsc. 1983; IV: 1683-1706.
(42) Reuter W. (1972) - The ionization function and its application to the electron probe analysis of thin films. 6th international conference on X-ray optics and microanalysis, Shinoda G., Kora K., Ichinokawa T. (eds), University of Tokyo Press, 121-130.
(43) Ruzakowski P., Holloway PH, Remond G. (1985) - Spatially resolved surface analysis using optical microreflectometry. J. Vac. Sci. Technol. A3, (3), May/June, 1380-1385.
(44) Rydnik VI, Borovskii IB. (1968) - Determining the thickness of composition of thin films with the aid of scattered electrons and characteristic x-ray radiation. Zavoadskaya Laboratoriya, 34(8), 1153-1158 (translation from Russian).
(45) Simpson PR, Cope MT. (1977) - Reference reflectance data for chalcocite, Internatl. Mineralogical Assoc., Commission on Ore Microscopy, Quantitative data file. The Applied Mineralogy Group of the Mineralogical Society, 41 Queen's Gate, London, England, card number 1.1460.
(46) Stern RM. (1974) - The backscattering of electrons by crystals at low and high energy. Appl. Phys. 9, 377-384.
(47) Tomlin SG. (1968) - Optical reflection and transmission formulae for thin films. Brit. J. Appl. Phys. (J. Phys., D.) Ser. 2, 1, 1667-1671.
(48) Trodahl HJ. (1984) - Optical adsorption in thin films. J. Phys.E: Sci. Instrum., 17, 27-29.
(49) Wright WD. (1964) - The measurement of colour, Hilger and Watts Ltd., London, 1-291.

## Discussion with Reviewers

M.F. Hochella Jr.: Does the reflectance data derived from the literature and used in this paper take into account actual surface compositions and layer thicknesses of the minerals measured?

W. Petruk: Since polishing introduces a surface layer on the substrate, and since this surface layer is different for each polishing method; is it technically sound to use reflectance measurements as a mineral identification tool, or should the measurements be used for scientific purposes?

Authors: As we have pointed out earlier, the reference data taken from the literature to derive optical constants probably had reaction products on the surfaces from which they were taken. As a result they are affected by surface layers of an unknown thickness and composition. This, of course, causes some ambiguity in our approach since our reference chalcopyrite data are already modified by surface reaction products. As a result, our reference constants are only effective constants equivalent to clear chalcopyrite with minimum iron oxide/copper rich sulfide layer thicknesses. These data agreed well with our present experimental reflectances of chalcopyrite polished with chromic oxide. Our experimental reflectance curves for freshly polished oxides and sulfides are consistent with published reflectance curves and the method remains a useful identification tool until the specimen preparation is carefully controlled.

M.F. Hochella Jr.: What evidence is there that surface composition changes result from temperature increases during polishing?

Authors: The evidence for increased temperature causing thicker reaction layers on chalcopyrite is indirect. First, it is obvious from touching the samples after diamond polishing that they are heated by the polishing. Second we have heated samples in air by a furnace and determined that the reaction layers thicken. These two qualitative observations led us to the postulate.

M.F. Hochella Jr.: In Fig. 11, the difference between curves 1 and 3 is sometimes more than half of the difference between curves 1 and 2. Does this not cast doubt on the reproducibility of the experimental reflectance curves?

Authors: While it is quite true that we have some experimental error in measuring the reflectances from surfaces, in general we have a precision of 1% reflectance for the same sample polished several different times. In general, surface reactions change the % reflectance by magnitudes greater than this precision, thereby proving that we are sufficiently accurate to draw conclusions.

M.F. Hochella Jr.: From this study of chalcopyrite, is it possible to at least partially extend these findings of the effect of surface composition and layer thickness upon reflectance to the most common and widespread of the sulfides, pyrite?

Authors: Since pyrite is a cubic material with isotropic optical properties, we anticipate no problem in using optical microreflectometry to study its surfaces.

J.S. Walker: What were the instruments used for the optical reflectance measurements, and were there any modifications made to them?

Authors: Two microreflectometers have been used in our studies, but the data for this study were mainly acquired from the instrument at BRGM. This instrument is described in details in reference 5 and in a paper submitted to Surface and Interface Analysis ( Application of experimental and calculated reflectance curves to the study of layered samples: An example of $SiO_x$ on InSb, by G.Remond et al. ). The light source, monochromator, microscope and detectors are shelf items with no extensive modifications being required.

J.S. Walker: How likely is it for thin film coatings to confuse mineral identification?

Authors: This good general question has the possibility of several answers. First, the reference optical data in the literature, upon which mineral identification is based, were all taken from samples which probably had reaction products on the surface. Second, the degree of confusion from thin film coatings will depend upon the properties of substrate and coating. For example, we have seen copper sulfide layers covering sphalerite substrates which have made it impossible to identify the underlying ZnS. Finally, severely tarnished surfaces can easily cause confusion. This is especially true when automated equipment ( rather than experienced mineralogists ) is used for mineral analysis. This again, emphasizes the need to study freshly polished surfaces.

J.S. Walker: Is it likely that thin film coatings could create significant problems in the use of automated reflectance and image analysis systems, given the sensitivity of conventional TV cameras or other imaging devices?

Authors: See the answer to question above. The use of an increased number of grey levels will be necessary to try to reduce the possibility of error.

Reviewer 3: I am frequently surprised by the poor quality of the polishing shown on the authors' polished sections ( e.g., Fig. 12 ). They are full of scratches; is there any explanation for this?

Authors: The polished surface shown in Fig. 12 is that of a sample first polished with diamond powder, then repolished for two minutes with chromic oxide. The chromic oxide polishing was stopped after two minutes ( rather than the normal twenty minutes ) to show that contrast was observed from removal of the thicker oxide/copper-rich sulfide layers induced by diamond polishing. The"scratches" referred to by the reviewer is simply a contrast resulting from differences in the reaction product thickness, and as discussed in the text, one can see how polishing is proceeding to remove the thicker reaction products. Also as pointed out in the text, this contrast cannot result from a real scratch on the surface which would imply differences in the surface topography. Real scratches were observed after prolonged polishing with soft cloth and chromic oxide. This is shown in Fig. 20b where numerous repolishing was necessary to accumulate the data. In general, poorly polished surfaces were avoided in our study.

Reviewer 3: Could the authors provide some direct evidence to prove the existence of a $Cu_5FeS_4$ film on the surface of the chalcopyrite? For example, any Auger electron spectroscopy, ESCA study, etc. One could possibly derive a calculated reflectance value similar to the observed value by adjusting the thickness, the composition and the number of layers. Is it possible to coat the fresh chalcopyrite with thin films of known materials and of known thickness, and compare the calculated with the observed reflectance values?

Authors : Relative to the last part of the question, we have checked our model against $SiO_2$ and $SiO_x$ layers deposited onto InSb substrates. Good agreement between calculated and experimental data supports the validity of our model. Relative to proof for the existence of $Cu_5FeS_4$ under the iron oxide layer, it is difficult to absolutely identify the sulfide layer. Auger and ESCA data show the layer is copper-rich, but the chemical shifts in either technique are not sufficient to identify bornite vs chalcocite, covellite, or several other copper-rich sulfides. Therefore we believe the reflectance measurements are as definitive as AES or ESCA data, but none absolutely establish the identity of the copper-rich sulfide.

Reviewer 4: It is not clear from the text whether the chalcopyrite crystals were analysed for trace element contents or compositional or structural zoning prior to use in this study. Small amounts of other elements will change the reflection behavior of chalcopyrite (e.g. the addition of Se will alter the color strongly towards brown ). Structural zoning or differences in orientation could be easily checked by etching with acid. Chalcopyrite samples from most types of lower temperature ore deposits including MVT deposits, some massive sulfides and sedimentary deposits will have a chemical composition close to $CuFeS_2$ but might have some natural zoning that would affect the optical properties and the average atomic number of the material. These effects may be small compared to the optical differences found for the tarnishing effects but they may account for some backscattered and secondary electron effects. Natural samples from higher temperature environments would have higher minor element contents, some of which may be exsolved on a very fine scale. The relationship between surface chemistry and trace element content in chalcopyrite should be considered.

Authors: Trace element analyses were carried out with the EPMA. Particular attention was given to As, Se, In and Ag. The primary beam energy was 30 keV, the beam intensity was 60 nA and the counting time was 60s for peak and background intensity measurements respectively. None of the above impurity was detected. The statistical limits of detection were 270 ppm for As, 200 ppm for Ag and In and 170 ppm for Se. These concentration levels are not expected to result in variations in either optical or secondary electron images. Furthermore, no zoning was detectable in either the SEM, EPMA and SAM. Finally, the question of a relationship between trace elements and surface chemistry is of extreme importance. We are continuing to investigate aspects of this question, but the present paper was intended to summarize a model which provides a basis for optical studies of this question. Therefore, a complete answer for this fundamental question is beyond the scope of this paper.

Reviewer 4: Under what storing conditions was the reflectance behavior least effected ( i.e., what method resulted in the least amount of tarnishing )? After polishing were they dried in air, in an oven, stored in a desiccator, under vacuum? These are practical hints which most ore microscopists would find useful for preparing and storing important samples and for evaluating the results of this study.

Authors: The first significant comment relative to this important question is that the thin oxide and copper-rich sulfide layers observed after polishing cannot be avoided; these reaction products form essentially instantaneously and will always be present. However, the layers were thicker after diamond as compared to chromic oxide polisher, therefore polishing technique with lower thermal effects should be prepared. The mechanism(s) causing thickening of the reaction layers is not well defined. It appears that temperature, moisture and contact with other minerals are all important. Storage at lower temperature in dry air ( i.e., a desiccator ) reduces the rate of growth of these layers in general. When moist air is the storage medium, we have observed transfer of elements from one mineral to the surface of the adjacent mineral. Again, storage in dry air would reduce this effect. We have also observed transport of silver across the surface due to photolytic decomposition of acanthite ( see e.g., reference 38 ) so reduced light intensity during optical microscopy may sometimes be necessary. But most important, analysis of polished samples should be performed with a minimum of delay.

Reviewer 4: The effect of orientation of the chalcopyrite on the reflection behavior is important when dealing with natural samples because a microscopist often has no control over this property when dealing with minerals in a thin section or polished mount. In your estimation, under what conditions is the ability to identify surface oxidation products using reflectance curves most enhanced? Under what conditions is it most limited?

Authors: This question is important in a general sense because the effects of reaction products upon the reflectance cannot always be separated from anisotropic optical properties ( see Table 2 ). But specifically for chalcopyrite, the anisotropy of the optical constants cause a maximum change in reflectance of 1% or less. This is within the accuracy of our measurement and is well below the changes caused by tarnishing; therefore it has no effect upon the current discussion.

Reviewer 4: The model developed for calculating reflectance curves for polished chalcopyrite with thin surface compounds incorporates the effects of multiple thin surface layers of absorbing material covering a substrate of absorbing material. The thin surface layers are assumed to be regular in thickness. In natural samples of chalcopyrite, oxidation may vary in thickness across a surface. How does this effect the application of your model?

Authors: Variation in the layer thickness over dimensions greater than 20 μm can be studied by selecting the area to be analyzed. However, when the thickness varies over dimensions below 10 μm, the measured intensity averages the effects of these variations. Our data show that for films of thickness lower than 20 nm, the reflectance at a given wavelength varied linearly with thickness ( see Fig. 9). Thus, the resultant reflectance would give the average thickness of the reaction product layers. Variations in thickness over dimensions<20 μm can also be analyzed using the heterogeneous rather than the homogeneous layer model. Again, below 20 nm, these models give the same curves. For layers thicker than 20 nm, the heterogeneous model should still give the average layer thickness.